
ECG-Reasoning-Benchmark: A Benchmark for Evaluating Clinical Reasoning Capabilities in ECG Interpretation

Jungwoo Oh¹, Hyunseung Chung¹, Junhee Lee¹, Min-Gyu Kim²
Hangyul Yoon¹, Ki Seong Lee¹, Youngchae Lee³ Muhan Yeo⁴, Edward Choi¹

¹KAIST ²Ajou University School of Medicine

³Yonsei University College of Medicine ⁴Seoul National University Bundang Hospital

¹{ojw0123, hs_chung, ciel3486, hangyulmd, kistar12, edwardchoi}@kaist.ac.kr

²manjmin6@gmail.com, ³dudco5307@yuhs.ac, ⁴smfforsm@gmail.com

Abstract

While Multimodal Large Language Models (MLLMs) show promising performance in automated electrocardiogram interpretation, it remains unclear whether they genuinely perform actual step-by-step reasoning or just rely on superficial visual cues. To investigate this, we introduce **ECG-Reasoning-Benchmark**, a novel multi-turn evaluation framework comprising over 6,400 samples to systematically assess step-by-step reasoning across 17 core ECG diagnoses. Our comprehensive evaluation of state-of-the-art models reveals a critical failure in executing multi-step logical deduction. Although models possess the medical knowledge to retrieve clinical criteria for a diagnosis, they exhibit near-zero success rates (< 6% Completion) in maintaining a complete reasoning chain, primarily failing to ground the corresponding ECG findings to the actual visual evidence in the ECG signal. These results demonstrate that current MLLMs bypass actual visual interpretation, exposing a critical flaw in existing training paradigms and underscoring the necessity for robust, reasoning-centric medical AI. The code and data are available at <https://github.com/Jwoo5/ecg-reasoning-benchmark>.

1 Introduction

Over the past decade, deep learning has revolutionized automated electrocardiogram (ECG) interpretation. Discriminative models have achieved diagnostic accuracy comparable to, and occasionally surpassing, human cardiologists in classification tasks [23, 19]. However, clinical practice remains hesitant to adopt these models. In the high-stakes domain of healthcare, a “black-box” prediction is insufficient. Clinicians require not just a diagnostic label, but the clinical reasoning and evidence that justify the conclusion to make informed decisions.

To bridge this interpretability gap, the field has rapidly pivoted toward Multimodal Large Language Models (MLLMs). Recent works such as PULSE [18], GEM [15], OpenTSLM [16], and ECG-R1 [12] integrate ECG signals with Large Language Models (LLMs) to generate diagnostic reports or answer clinical queries. While these models can generate fluent and plausible-sounding explanations, they introduce a new and dangerous risk: hallucination. This risk of hallucination fundamentally stems from how their training data is constructed. In many existing datasets, the training explanations are synthetically generated by providing an LLM like GPT-4 [1] with the final diagnostic labels and machine-generated reports, typically without direct exposure to the actual ECG signal. Because the models are trained on these text-derived rationales rather than visually grounded features, they often struggle to ground their interpretations to raw physiological evidence. Instead, they learn to

generate medically fluent justifications that recite textbook descriptions associated with the diagnosis, regardless of what the underlying signal actually shows.

Furthermore, the prevailing evaluation methodology worsens this disconnect. Existing studies predominantly rely on the LLM-as-a-Judge framework [33], which evaluates the generated interpretation by comparing it against a reference response. A major limitation of this approach is that these reference explanations are also synthetically created by an LLM. Therefore, measuring the alignment between a model’s output and these references primarily assesses how well the model mimics the linguistic style of the text generator. Because the judge-LLM never looks at the actual ECG image to verify the model’s response, this framework can validate whether an explanation is medically plausible and fluent, but cannot verify if the interpretation is grounded in the underlying ECG signal.

To address these limitations in current evaluation paradigms, we propose **ECG-Reasoning-Benchmark**. We posit that evaluating an ECG-MLLM should not be a test of fluency, but a rigorous “clinical reasoning exam” that probes the model’s intrinsic reasoning capabilities. We conceptualize ECG interpretation as a multi-stage deduction process requiring established medical knowledge, perceptual detection, and precise visual grounding of ECG features. To rigorously assess this process, we implement a 4-stage verification loop that sequentially evaluates the reasoning trajectory from initial criterion selection to the final diagnostic decision.

Our contributions are summarized as follows:

1. We propose **ECG-Reasoning-Benchmark**, a novel evaluation framework grounded in established clinical criteria and precise ECG features. This shifts the evaluation paradigm from subjective LLM-as-a-Judge scoring to rigorous step-by-step verification, providing a reliable standard to ascertain whether models base their decisions on the actual ECG signal.
2. To facilitate this rigorous evaluation, we develop a comprehensive automated ECG analysis pipeline that extracts explicit diagnostic features directly from raw 12-lead signals. By progressively mapping wave delineations and quantitative measurements to discrete clinical findings, this tool establishes a transparent and objective ground truth for the clinical reasoning chains required for our benchmark.
3. Through a comprehensive evaluation of state-of-the-art MLLMs, we reveal a critical failure in multi-step logical deduction. We demonstrate that while current models possess the medical knowledge to identify which ECG findings are required for a diagnosis, they critically lack the capability to ground those specific findings within the ECG signal. These findings indicate that existing models bypass actual visual interpretation, highlighting a current limitation in their visual grounding capabilities.

2 Related Works

The initial wave of ECG-MLLMs focused on adapting general-purpose vision-language architectures to the cardiac domain. Early initiatives such as MEIT [30], ECG-LM [31], and Q-Heart [22] treated ECG interpretation as a translation task, mapping global signal embeddings to clinical reports (*i.e.*, report generation task) or text-based answers (*i.e.*, question answering task). While effective for these specific tasks, they still lack the capacity to explain the grounded evidence underlying their outputs.

Subsequent research attempted to bridge this gap by incorporating explicit reasoning processes into both models and datasets. However, they fundamentally rely on synthetic data generation processes. For instance, PULSE [18] is fine-tuned on the ECGInstruct dataset, where instruction-response pairs were synthesized by Llama-3-70B-Instruct [7] without direct exposure to actual signals. Recognizing the need for structural grounding, later efforts attempted to incorporate physical measurements extracted from an external tool [8, 9]. GEM [15] introduced the ECG-Grounding dataset, and ECG-R1 [12] utilized the ECG-Protocol-Guided-Grounding-CoT dataset. Meanwhile, OpenTSLM [16] employed the ECG-QA-CoT dataset, which relies on Chain-of-Thought trajectories generated by GPT-4o [10] from question-answer pairs in the ECG-QA dataset [21]. Other approaches like ECG-Chat [32] integrated Retrieval-Augmented Generation to mitigate hallucination.

Despite these advancements, a fundamental limitation persists in these methodologies due to their reliance on synthetic ground truth. Because the reasoning chains in these works are synthesized by LLMs, trained models learn to emulate the linguistic style of the teacher model rather than deriving evidence from the raw signal. Furthermore, the prevailing LLM-as-a-Judge evaluation frameworks

cannot verify whether the interpretations are actually supported by the input signal. To address these structural limitations, our **ECG-Reasoning-Benchmark** provides an objective and quantitative examination of explicit clinical reasoning grounded in the ECG signal.

3 Automated ECG Analysis Pipeline

To facilitate a rigorous reasoning benchmark, it is imperative to establish a ground truth that provides a transparent and traceable chain of clinical evidence. However, such granular annotations are largely absent from existing public ECG datasets, which typically provide high-level diagnostic labels without the exact waveform boundaries or specific interval measurements required for clinical reasoning. To overcome this, we developed an **Automated ECG Analysis Pipeline**, which constructs verifiable ground-truth annotations by systematically extracting physiological evidence directly from the raw signal. To provide a clear overview of this systematic extraction process, the schematic illustration of this pipeline is provided in Figure 1.

3.1 Wave Detection and Segmentation

The foundation of the pipeline lies in the precise delineation of the P wave, QRS complex, and T wave. To achieve this, we employ a U-Net3+ architecture [13] to perform the initial wave detection. For a given 12-lead ECG, the model processes each lead individually, generating separate probability maps for four classes: P wave, QRS complex, T wave, and the isoelectric background. To refine these initial outputs for the clinical validity, we further apply context-aware post-processing algorithms:

- **P-wave recovery via template matching:** We observed that deep-learning-based models often fail to detect non-conducted P waves that appear without a subsequent QRS complex (*e.g.*, in high-degree AV blocks). To address these missed detections, the pipeline performs a secondary search within RR intervals where no P waves were initially identified. This targeted search utilizes SciPy’s [28] peak detection algorithm on the unannotated segments, guided by a “P wave template” derived from the average duration and amplitude of successfully detected P waves within the same lead. Specifically, candidate peaks are validated based on two criteria: (1) physiological constraints, requiring a minimal duration of 60 ms and an amplitude exceeding a noise threshold (5% of the adjacent QRS amplitude), and (2) morphological similarity to the established template (*i.e.*, sharing the identical positive, negative, or biphasic deflection).
- **Physiological constraint enforcement:** We apply strict biological rules to eliminate artifacts, such as ensuring each cardiac cycle contains only one T-wave following a QRS complex. Multiple T wave candidates within a single RR interval are resolved by selecting the most probable peak based on its timing relative to the QT interval.
- **Multi-lead consensus alignment:** To account for lead-specific noise, we implement a 4-lead consensus rule. A wave is validated only if it is detected at a consistent temporal location in at least 4 of the 12 leads. Once validated, global boundaries are defined by the earliest onset and latest offset across the contributing leads to capture the full duration of the corresponding waves.

Given that precise wave delineation is the critical foundation for all subsequent ECG analysis, we evaluated the performance of this detection module. Specifically, empirical evaluations on the Lobachevsky University Electrocardiography Database (LUDB) [14] indicate that our pipeline provides robust detection accuracy compared to traditional signal processing baselines. The pipeline achieves an average recall and precision of 1.000 for QRS complexes, 0.978 and 0.937 for P waves, and 0.996 and 0.992 for T waves. Detailed results are provided in Appendix A.1.

3.2 Feature Extraction

Quantification Following the precise segmentation of waveforms, the pipeline proceeds to a hierarchical feature extraction phase. The cornerstone of this analysis is the quantification of low-level ECG features. This includes temporal measurements such as the duration of P, QRS, and T waves, alongside important physiological intervals like PR, RR, and QT intervals. Simultaneously, amplitude measurements are computed by measuring peak heights relative to the isoelectric line and quantifying ST-segment deviations at the J-point. To capture subtle conduction abnormalities, the pipeline also performs a detailed morphological analysis, identifying specific QRS structural configurations such as qR, rS, and RSR’ patterns, as well as explicitly verifying the presence of



Figure 1: End-to-end schematic of the Automated ECG Analysis Pipeline. The workflow illustrates a systematic progression: from the initial delineation of fundamental waveforms in the raw signal to the quantification of physiological features, which are then mapped into discrete clinical findings and ultimately resulting in a definitive diagnostic conclusion.

pathological Q waves. Additionally, we compute the frontal plane electrical axis for each beat based on the net area under the QRS complexes in leads I and aVF.

Finding Extraction Once these continuous quantitative measurements are extracted, the pipeline proceeds to map them to ECG findings. This step bridges the gap between raw signal processing and medical terminology by applying established clinical criteria. For instance, continuous interval values are evaluated against standard physiological limits, where a PR interval exceeding 200 ms in the majority of detected beats is formally identified as a “Prolonged PR interval”. This transformation converts the dense, high-dimensional feature space into a discrete set of interpretable clinical findings.

Diagnosis Derivation The final stage of the pipeline combines these identified findings to establish a clinical diagnosis. To ensure clinical validity, we constructed a hierarchical logic diagrams covering 17 core ECG diagnoses, codified from authoritative guidelines such as the ECG Core Curriculum [34] and were further validated by three board-certified internal medicine specialists. The complete set of logic diagrams for all diagnoses is provided in Appendix A.2. This strict framework enforces a diagnosis to be confirmed only when a specific, clinically valid combination of findings is present. By structuring the analysis in this manner, we generate a ground truth that explicitly details the causal chain of evidence, thereby enabling the rigorous verification of the model’s reasoning process.

4 Construction of ECG-Reasoning-Benchmark

Leveraging the structured ground truth derived from our automated pipeline, we constructed **ECG-Reasoning-Benchmark**. Distinct from traditional QA datasets, and diverging from recent reliance on subjective LLM-as-a-Judge approaches, our framework provides an objective testbed that verifies whether each step in the entire chain of clinical deduction is grounded in physical signal evidence.

4.1 Evaluation Workflow

Inspired by the methodology of CXReasonBench [17], our evaluation protocol begins with an Initial Diagnostic Question (*e.g.*, “Does this ECG suggest the presence of first-degree AV block?”). This

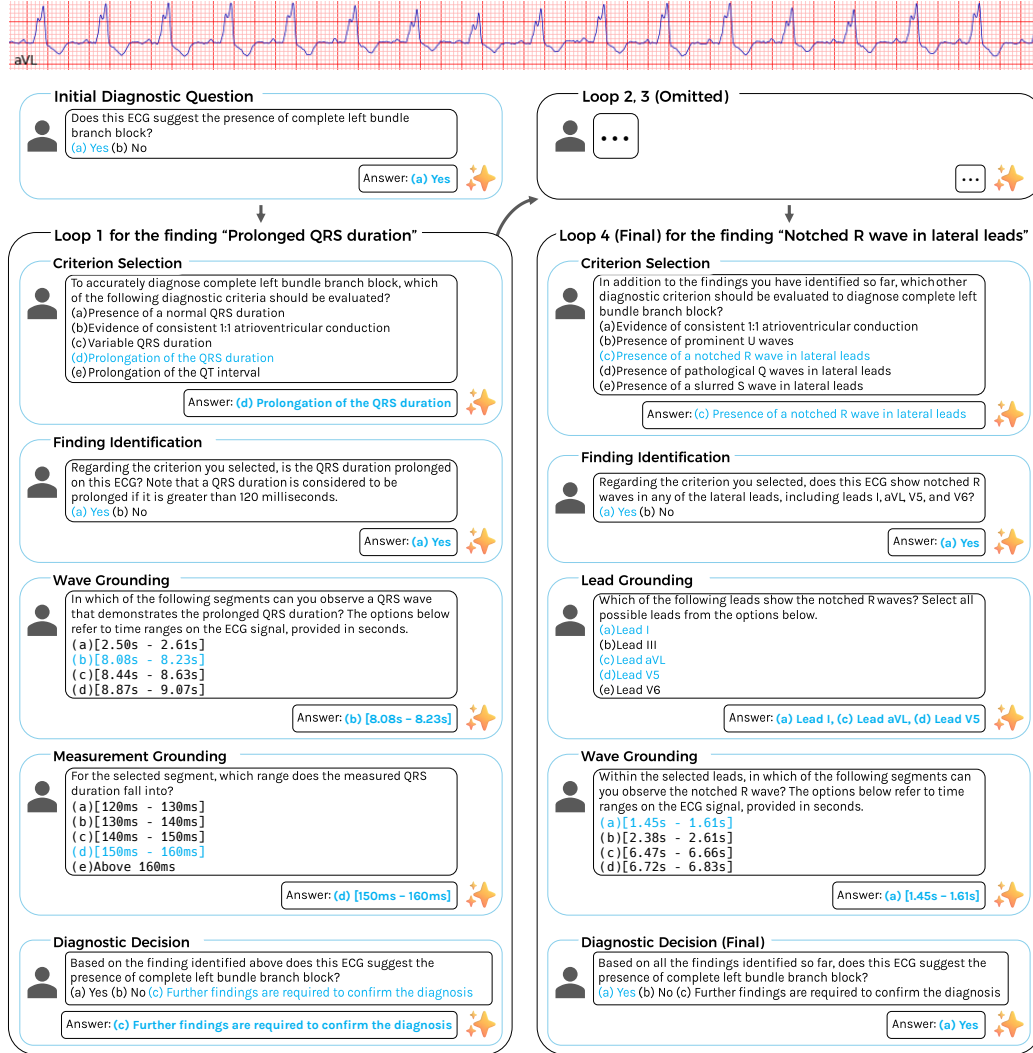


Figure 2: An illustrative example of the 4-step recursive evaluation loop for diagnosing Complete Left Bundle Branch Block. The process begins with an Initial Diagnostic Question, followed by the verification of necessary findings. The figure depicts the first loop, which verifies the presence of “Prolonged QRS duration” grounded in the wave segment and measurement range, and the fourth loop, which confirms the “Notched R wave in lateral leads” with specific lead and wave grounding.

step establishes a baseline for the model’s intuitive diagnostic capability prior to engaging in detailed reasoning. Importantly, regardless of whether the model answers this initial question correctly, the evaluation advances to the step-wise verification process described in the following paragraph.

Following this initial query, we evaluate the model’s reasoning capability through a step-wise verification process, which systematically challenges the model to execute the rigorous chain of clinical deduction required for the diagnosis. The verification process for each individual clinical finding comprises four distinct steps, structured as follows:

1. **Criterion Selection:** The model must first identify the specific diagnostic criterion relevant to the target diagnosis (e.g., “To accurately diagnose complete left bundle branch block, which of the following diagnostic criteria should be evaluated?”). To strictly evaluate discriminatory ability, we employ two types of distractors comprising of category-based and presence-based distractors. Specifically, category-based distractors introduce incorrect options drawn from the same clinical category as the correct finding (e.g., contrasting “Prolonged PR interval” with “Normal PR interval”). On the other hand, presence-based distractors consist of findings that are present in the current ECG recording but are clinically irrelevant to the diagnosis in question.

2. **Finding Identification:** Upon selecting a criterion, the model is challenged to verify its presence in the current recording (*e.g.*, “Is the QRS duration prolonged on this ECG?”). This assesses the model’s fundamental perceptual capacity to detect abnormalities visually.
3. **ECG Grounding:** To distinguish genuine analysis from hallucination, we demand explicit signal grounding, which involves three granular sub-tasks:
 - **Lead Grounding:** For findings associated with specific anatomical regions or lead groups, the model must identify the precise leads exhibiting the abnormality (*e.g.*, “Which of the following leads show the notched R waves?”).
 - **Wave Grounding:** The model is required to temporally locate the relevant waveforms within the 10-second strip to demonstrate its visual focus (*e.g.*, “In which of the following segments can you observe the notched R wave?”).
 - **Measurement Grounding:** The model quantifies the specific feature by selecting the correct value range (*e.g.*, “Which range does the measured QRS duration fall into?”)
4. **Diagnostic Decision:** Finally, based on the verified findings, the model determines whether the diagnosis can be confirmed or if “further findings are required” (*e.g.*, “Based on all the findings identified so far, does this ECG suggest the presence of complete left bundle branch block?”).

This 4-step validation sequence is applied iteratively for every clinical finding required to support the diagnosis. That is, for diagnoses defined by a combination of multiple criteria, the model is required to successfully navigate this verification loop for each individual finding in succession. Consequently, the final diagnostic conclusion is reached only after the model has explicitly validated every piece of supporting evidence through this exacting cycle. An example for diagnosing Complete Left Bundle Branch Block is visually provided in Figure 2. The constituent criteria and their hierarchical arrangement are derived from the verified logic diagrams described in Section 3.2.

4.2 Sampling Strategy

To ensure the benchmark serves as a robust and unbiased evaluator of clinical reasoning, we implemented a sophisticated sampling strategy. Specifically, we curated a balanced set of 100 positive and 100 negative samples for each of the 17 core diagnoses. Crucially, since a single diagnosis can be confirmed through multiple combinations of clinical findings, we ensured that the selected samples were evenly distributed across the various logical paths defined in our logic diagrams. This approach enables the benchmark to evaluate the model’s competence across diverse clinical presentations.

To further guarantee the reliability of the ground truth, we strictly filtered the dataset to include only samples where the provided human label aligns with our automated pipeline’s diagnosis. This verification process ensures that every sample is not only labeled by a human expert but also quantitatively supported by verifiable signal features. Applying this protocol to two source datasets, PTB-XL [29] and MIMIC-IV-ECG [6], we constructed a comprehensive benchmark comprising over 6,400 samples (3,076 from PTB-XL and 3,355 from MIMIC-IV-ECG), where the detailed dataset statistics can be found in Appendix B.

Finally, three board-certified internal medicine specialists validated 143 representative samples to establish a reliable baseline for data quality. This subset was constructed by sampling one instance per unique reasoning path from both PTB-XL and MIMIC-IV-ECG, excluding one rare path unavailable in PTB-XL. Following this expert verification, all authors manually reviewed the extracted reasoning path for every single sample, under the supervision of the specialists to ensure the dataset integrity.

5 Experiments

5.1 Experimental Setup

Evaluated Models To comprehensively assess clinical reasoning capabilities, we evaluate a diverse suite of state-of-the-art Multimodal Large Language Models (MLLMs) processing either visual or time-series inputs. Our evaluation includes ECG-specific models (PULSE [18], GEM [15], ECG-R1 [12], OpenTSLM [16]), medical-domain models (Hulu-Med [11], MedGemma [24]), open-weight general domain models (Qwen3-VL [3], Llama-3.2-Vision [7]), and proprietary models (Gemini-2.5-Flash [4], Gemini-2.5-Pro [4], Gemini-3-Flash [26], GPT-5-Mini [25], GPT-5.2 [25]). Detailed model configurations are provided in Appendix C.

Data Processing Depending on the architectural requirements of each model, the ECG data is inputted either as 1D time-series arrays or 2D images. Specifically, for OpenTSLM, which is natively designed for time-series, the input is provided as a 100Hz, 12-channel time-series signal. For all other vision-capable models, the 1D signals are converted into standard 12-lead 2D ECG images using the `ecg-plot` Python package. Additionally, to ensure a fair evaluation, we provide a system prompt that instructs the models to strictly follow authoritative clinical guidelines and standard diagnostic criteria. This design aligns the models with our evaluation framework, which requires a complete verification of all findings before reaching a final diagnosis. Accordingly, this approach prevents models from being unfairly penalized for premature diagnoses, and ensures a consistent assessment of their systematic reasoning capabilities. The system prompts are presented in Appendix C.3.

Evaluation Metrics The evaluation is conducted in a multi-turn conversational format to systematically assess the model’s step-by-step reasoning process. Rather than relying on rigid string matching, which often penalizes correct answers formulated in different styles, we employ Gemini-3-Flash [26] to verify the semantic consistency between the models’ response and the ground truth answer at every step. We quantify the models’ reasoning capabilities using the following metrics:

- **Initial Diagnosis Accuracy (IDA) (%)**: Measures the model’s baseline diagnostic accuracy based solely on the Initial Diagnostic Question, prior to engaging in any step-wise reasoning.
- **Completion (%)**: A strict metric representing the proportion of samples where the model correctly answers every constituent multi-turn reasoning question. Because the evaluation for this metric terminates upon the first incorrect response at any reasoning step, it reflects the model’s ability to navigate the entire causal chain without a single logical or perceptual failure.
- **Depth (0-4)**: Quantifies the model’s average progression through the 4-step verification sequence, evaluated independently per finding. For this metric, if a model fails at any step within a finding loop, its depth score for that finding is recorded, and the evaluation proceeds to the next required finding by providing the ground-truth history of all preceding steps in the prompt. These finding-level depths are then pooled across all samples to calculate the global average. This ensures that every necessary finding is independently evaluated, allowing us to measure which stage the models can successfully reach on average. Within each finding, Step 3 (ECG Grounding) is scored fractionally based on its N required sub-tasks (*i.e.*, Lead, Wave, and Measurement Grounding), where each correctly answered sub-task contributes $1/N$ to the depth score. To provide further clarity on this scoring mechanism, a concrete step-by-step example of the Depth calculation is presented in Appendix C.1.
- **GT-Reasoning-Based Diagnosis Accuracy (GT-RDA) (%)**: Assesses the model’s diagnostic performance under the guidance of a perfect reasoning trajectory. For this metric, regardless of any prior failures at earlier steps, we explicitly provide the complete ground-truth reasoning history up to the final Diagnostic Decision step in the prompt, and then assess the accuracy of this final step. By comparing this accuracy with the Initial Diagnosis Accuracy, we measure the model’s capacity to comprehend and leverage the provided reasoning process.

5.2 Results

Evaluation of Reasoning Completion Table 1 highlights a significant limitation in the models’ ability to sustain a complete chain of clinical reasoning. Across all evaluated models and both datasets, performance on the **Completion** metric is remarkably poor, with maximum success rates reaching only around 6% (*e.g.*, Gemini-3-Flash achieving 6.26% on PTB-XL, and ECG-R1-RL achieving 5.81% on MIMIC-IV-ECG). Notably, despite being explicitly tailored to the medical or ECG domains, smaller open-weight models such as OpenTSLM (3B), MedGemma (4B), and MedGemma-1.5 (4B) fail almost entirely, demonstrating completion rates around or below 1%. A qualitative review of their responses reveals that these compact models frequently lose contextual focus during the multi-turn verification loops, generating irrelevant or repetitive responses. This suggests that their limited parameter capacity restricts their ability to maintain sustained logical reasoning. Interestingly, a similar result is observed in Llama-3.2-Vision (11B), which underperforms smaller 8B models such as Qwen3-VL. We speculate that the failure of this model stems from a lack of exposure to ECG or medical contexts during its training phase. Conversely, the robust performance of Qwen3-VL implies that its training corpus encompassed substantial medical or ECG-specific data.

Table 1: Quantitative benchmark results of the evaluated models on **ECG-Reasoning-Benchmark** across both PTB-XL and MIMIC-IV-ECG source datasets. Models are grouped into ECG-specific, medical domain, general domain, and proprietary categories, with the highest score for each metric highlighted in bold within its respective source dataset.

Source Dataset	Model	IDA (%)	Completion (%)	Depth (0-4)	GT-RDA (%)
PTB-XL	PULSE (7B) [18]	80.93	5.45	1.24	35.18
	GEM (7B) [15]	84.37	6.13	1.34	65.66
	ECG-R1-SFT (8B) [12]	85.12	5.45	1.80	21.76
	ECG-R1-RL (8B) [12]	85.41	5.90	1.79	22.70
	OpenTSLM (3B) [16]	54.77	0.65	0.17	37.58
	Hulu-Med (7B) [11]	55.87	4.96	1.20	86.87
	Hulu-Med (32B) [11]	57.49	3.21	1.62	99.42
	MedGemma (4B) [24]	52.59	0.58	0.80	33.24
	MedGemma (27B) [24]	55.19	1.20	1.51	76.46
	MedGemma-1.5 (4B) [24]	42.83	0.68	0.92	85.02
	Qwen3-VL (8B) [3]	52.85	5.67	1.53	85.80
	Qwen3-VL (32B) [3]	59.73	5.71	1.63	89.46
	Llama-3.2-Vision (11B) [7]	45.75	0.49	1.01	77.17
	Llama-3.2-Vision (90B) [7]	56.84	4.47	1.34	91.21
	Gemini-2.5-Flash [4]	57.75	5.12	1.83	89.69
	Gemini-2.5-Pro [4]	55.12	3.44	2.01	86.87
	Gemini-3-Flash [26]	65.86	6.26	2.09	91.76
	GPT-5-Mini [25]	57.85	2.37	1.75	78.18
	GPT-5.2 [25]	67.80	5.84	1.97	85.70
	MIMIC-IV-ECG	PULSE (7B) [18]	72.10	4.76	1.22
GEM (7B) [15]		76.27	5.30	1.30	57.01
ECG-R1-SFT (8B) [12]		79.58	5.45	1.71	22.12
ECG-R1-RL (8B) [12]		80.17	5.81	1.71	22.95
OpenTSLM (3B) [16]		51.56	0.36	0.13	35.43
Hulu-Med (7B) [11]		50.79	4.85	1.13	85.83
Hulu-Med (32B) [11]		51.62	3.36	1.53	97.20
MedGemma (4B) [24]		49.30	0.83	0.80	30.72
MedGemma (27B) [24]		50.88	1.22	1.45	78.24
MedGemma-1.5 (4B) [24]		46.98	1.01	0.95	84.52
Qwen3-VL (8B) [3]		53.53	5.45	1.54	86.19
Qwen3-VL (32B) [3]		54.30	5.03	1.59	88.00
Llama-3.2-Vision (11B) [7]		49.75	0.74	1.02	74.31
Llama-3.2-Vision (90B) [7]		52.52	4.38	1.27	88.39
Gemini-2.5-Flash [4]		53.74	4.91	1.78	89.73
Gemini-2.5-Pro [4]		54.69	3.81	1.98	88.06
Gemini-3-Flash [26]		60.64	5.72	2.07	91.25
GPT-5-Mini [25]		51.50	2.14	1.70	75.65
GPT-5.2 [25]		63.41	5.27	1.93	83.83

Depth Analysis The **Depth** metric isolates the exact stage where the models’ reasoning sequences collapse on average. Consistently across both datasets, with the exception of the smallest models (OpenTSLM (3B), MedGemma (4B), MedGemma-1.5 (4B)), nearly all evaluated models achieve an average depth greater than 1.0. This indicates a broad success in the first verification stage: **Criterion Selection**. The models successfully identify what clinical criteria must be evaluated to confirm a diagnosis (*e.g.*, retrieving the knowledge that a “Prolonged PR interval” is necessary for First-degree AV Block). However, average depth scores rarely exceed 2.0 across the board, pinpointing the critical bottleneck at the subsequent **Finding Identification** and **ECG Grounding** stages. Therefore, we suspect that while the current generation of AI models possesses the medical knowledge required for diagnosis, they lack the crucial ability to reliably ground that logic to the granular visual evidence of the ECG signal. This observation suggests that the primary limitation in automated ECG interpretation is not a knowledge deficit, but a profound reasoning gap in linking diagnostic criteria to the actual detection and measurement of specific findings within the signal.

IDA vs. GT-RDA Another notable insight of this benchmark emerges from the comparison of Initial Diagnosis Accuracy (IDA) and GT-Reasoning-Based Diagnosis Accuracy (GT-RDA). As a

baseline observation, excluding ECG-specific models, most evaluated models achieve an IDA of approximately 50%, indicating they are randomly guessing the initial diagnosis. However, for these non-ECG-specific models, providing the ground-truth reasoning trajectory yields the expected result, which is a massive surge in diagnostic accuracy across both datasets (*e.g.*, Hulu-Med (32B) soaring from 57.49% to 99.42% on PTB-XL and 51.62% to 97.20% on MIMIC-IV-ECG). This demonstrates their latent capacity to utilize valid evidence when perfectly guided. In contrast, the ECG-specific models exhibit a performance collapse when provided with the correct reasoning process. For instance, ECG-R1-RL achieves a high IDA (85.41% on PTB-XL and 80.17% on MIMIC-IV-ECG), yet its accuracy drops significantly under the GT-RDA evaluation (22.70% and 22.95%, respectively). PULSE similarly drops from 80.93% to 35.18% on PTB-XL and 72.10% to 30.01% on MIMIC-IV-ECG. This unexpected degradation exposes a critical flaw in current ECG-specific MLLMs, in that they have not learned to interpret ECGs through valid clinical reasoning. Instead, they appear to have optimized for a superficial pattern that links global signal patterns directly to high-level diagnostic conclusions. While training these models to generate interpretations may yield high subjective scores under the LLM-as-a-Judge framework, our benchmark empirically demonstrates that such approaches struggle to instill the genuine, step-by-step clinical deduction required for reliable ECG interpretation.

6 Discussion

This study addresses a critical blind spot in the evaluation of multimodal large language models for automated ECG interpretation. By introducing **ECG-Reasoning-Benchmark**, we shifted the evaluation paradigm from assessing superficial diagnostic accuracy based on LLM-as-a-Judge framework to rigorously verifying the underlying clinical deduction process. Our comprehensive analysis across a diverse suite of models uncovers a profound reasoning gap. We demonstrated that while current state-of-the-art models excel at generating plausible diagnoses, they fail to ground their logic to granular visual evidence in the ECG signal. Furthermore, the performance collapse observed in ECG-specific models when they are provided with ground-truth reasoning pathways suggests their reliance on superficial pattern-matching rather than valid medical deduction. Ultimately, our findings highlight that satisfying the linguistic evaluation of the LLM-as-a-Judge framework is insufficient to ensure the clinical reliability required for automated ECG interpretation. Future development in this domain must prioritize the implementation of transparent and verifiable step-by-step reasoning grounded in the physical signal to achieve trustworthy automated ECG interpretation.

Despite these contributions, we acknowledge several limitations in its current implementation.

The Exclusion of Diagnostic Uncertainty In real-world clinical practice, ECG interpretation inherently involves a degree of diagnostic uncertainty and ambiguity. However, to establish an indisputable ground truth for our benchmark, we intentionally excluded borderline or ambiguous samples through rigorous manual review to ensure the absolute reliability of the evaluation metrics. While this design choice provides a strict standard for assessing logical deduction, it limits the benchmark’s ability to evaluate how well models navigate clinical uncertainty. Future iterations of the automated ECG analysis pipeline aim to formalize the definition of uncertainty, allowing for the reintroduction of borderline cases. This will enable the valuation of a model’s capacity to recognize ambiguity and express appropriate diagnostic doubt, a critical skill for safe medical AI.

Structured Verification vs. Clinical Heuristics To systematically evaluate reasoning capabilities, our benchmark enforces a formalized, sequential reasoning process. While the finding sequences for each diagnosis are derived from textbook definitions and validated by board-certified internal medicine specialists, this structured multi-turn evaluation may not perfectly mirror the dynamic workflow of experienced clinicians. In practice, physicians frequently rely on clinical heuristics rather than exhaustively verifying every single criterion. For instance, if a diagnosis requires three distinct findings, but one finding presents with absolute certainty, a clinician might confidently confirm the diagnosis without explicitly evaluating the remaining findings. Currently, our benchmark requires the complete traversal of all associated findings, penalizing models that attempt such heuristic shortcuts. In future work, we plan to evolve our static reasoning pathways into dynamic reasoning diagrams by incorporating severity and certainty weightings for individual findings. This advancement would support an early termination evaluation scheme, where models are appropriately rewarded for confidently reaching a diagnosis based on highly certain, severe findings without redundant verification, thereby reflecting a more realistic and advanced level of clinical expertise.

References

- [1] Josh Achiam, Steven Adler, Sandhini Agarwal, Lama Ahmad, Ilge Akkaya, Florencia Leoni Aleman, Diogo Almeida, Janko Altschmidt, Sam Altman, Shyamal Anadkat, et al. Gpt-4 technical report. *arXiv preprint arXiv:2303.08774*, 2023.
- [2] Association for the Advancement of Medical Instrumentation. Ansi/aami ec57:1998/(r)2008 (revision of aami ecar:1987). American National Standard, 1999. Standard.
- [3] Shuai Bai, Yuxuan Cai, Ruizhe Chen, Keqin Chen, Xionghui Chen, Zesen Cheng, Lianghao Deng, Wei Ding, Chang Gao, Chunjiang Ge, et al. Qwen3-vl technical report. *arXiv preprint arXiv:2511.21631*, 2025.
- [4] Gheorghe Comanici, Eric Bieber, Mike Schaekermann, Ice Pasupat, Noveen Sachdeva, Inderjit Dhillon, Marcel Blistein, Ori Ram, Dan Zhang, Evan Rosen, et al. Gemini 2.5: Pushing the frontier with advanced reasoning, multimodality, long context, and next generation agentic capabilities. *arXiv preprint arXiv:2507.06261*, 2025.
- [5] A. Goldberger, L. Amaral, L. Glass, J. Hausdorff, P. C. Ivanov, R. Mark, J. E. Mietus, G. B. Moody, C. K. Peng, and H. E. Stanley. PhysioBank, PhysioToolkit, and PhysioNet: Components of a new research resource for complex physiologic signals. *Circulation*, 101(23):e215–e220, 2000. RRID:SCR_007345.
- [6] Brian Gow, Tom Pollard, Larry A Nathanson, Alistair Johnson, Benjamin Moody, Chrystinne Fernandes, Nathaniel Greenbaum, Seth Berkowitz, Dana Moukheiber, Parastou Eslami, et al. Mimic-iv-ecg-diagnostic electrocardiogram matched subset.
- [7] Aaron Grattafiori, Abhimanyu Dubey, Abhinav Jauhri, Abhinav Pandey, Abhishek Kadian, Ahmad Al-Dahle, Aiesha Letman, Akhil Mathur, Alan Schelten, Alex Vaughan, et al. The llama 3 herd of models. *arXiv preprint arXiv:2407.21783*, 2024.
- [8] Shenda Hong, Meng Wu, Yuxi Zhou, Qingyun Wang, Junyuan Shang, Hongyan Li, and Junqing Xie. Encase: An ensemble classifier for ecg classification using expert features and deep neural networks. In *2017 Computing in cardiology (cinc)*, pages 1–4. IEEE, 2017.
- [9] Shenda Hong, Yuxi Zhou, Meng Wu, Junyuan Shang, Qingyun Wang, Hongyan Li, and Junqing Xie. Combining deep neural networks and engineered features for cardiac arrhythmia detection from ecg recordings. *Physiological measurement*, 40(5):054009, 2019.
- [10] Aaron Hurst, Adam Lerer, Adam P Goucher, Adam Perelman, Aditya Ramesh, Aidan Clark, AJ Ostrow, Akila Welihinda, Alan Hayes, Alec Radford, et al. Gpt-4o system card. *arXiv preprint arXiv:2410.21276*, 2024.
- [11] Songtao Jiang, Yuan Wang, Sibao Song, Tianxiang Hu, Chenyi Zhou, Bin Pu, Yan Zhang, Zhibo Yang, Yang Feng, Joey Tianyi Zhou, et al. Hulu-med: A transparent generalist model towards holistic medical vision-language understanding. *arXiv preprint arXiv:2510.08668*, 2025.
- [12] Jiarui Jin, Haoyu Wang, Xingliang Wu, Xiaocheng Fang, Xiang Lan, Zihan Wang, Deyun Zhang, Bo Liu, Yingying Zhang, Xian Wu, et al. Ecg-r1: Protocol-guided and modality-agnostic mllm for reliable ecg interpretation. *arXiv preprint arXiv:2602.04279*, 2026.
- [13] Chankyu Joung, Mijin Kim, Taejin Paik, Seong-Ho Kong, Seung-Young Oh, Won Kyeong Jeon, Jae-hu Jeon, Joong-Sik Hong, Wan-Joong Kim, Woong Kook, et al. Deep learning based ecg segmentation for delineation of diverse arrhythmias. *PLoS one*, 19(6):e0303178, 2024.
- [14] Alena I Kalyakulina, Igor I Yusipov, Viktor A Moskalenko, Alexander V Nikolskiy, Konstantin A Kosonogov, Grigory V Osipov, Nikolai Yu Zolotykh, and Mikhail V Ivanchenko. Ludb: a new open-access validation tool for electrocardiogram delineation algorithms. *IEEE access*, 8:186181–186190, 2020.
- [15] Xiang Lan, Feng Wu, Kai He, Qinghao Zhao, Shenda Hong, and Mengling Feng. Gem: Empowering mllm for grounded ecg understanding with time series and images. *arXiv preprint arXiv:2503.06073*, 2025.
- [16] Patrick Langer, Thomas Kaar, Max Rosenblattl, Maxwell A Xu, Winnie Chow, Martin Maritsch, Aradhana Verma, Brian Han, Daniel Seung Kim, Henry Chubb, et al. Opentslm: Time-series language models for reasoning over multivariate medical text-and time-series data. *arXiv preprint arXiv:2510.02410*, 2025.
- [17] Hyungyung Lee, Geon Choi, Jung Oh Lee, Hangyul Yoon, Hyuk Gi Hong, and Edward Choi. CXReasonBench: A Benchmark for Evaluating Structured Diagnostic Reasoning in Chest X-rays. *PhysioNet*, October 2025. Version 1.0.1.

- [18] Ruoqi Liu, Yuelin Bai, Xiang Yue, and Ping Zhang. Teach multimodal llms to comprehend electrocardiographic images. *arXiv preprint arXiv:2410.19008*, 2024.
- [19] Xinwen Liu, Huan Wang, Zongjin Li, and Lang Qin. Deep learning in ecg diagnosis: A review. *Knowledge-Based Systems*, 227:107187, 2021.
- [20] Dominique Makowski, Tam Pham, Zen J. Lau, Jan C. Brammer, François Lespinasse, Hung Pham, Christopher Schölzel, and S. H. Annabel Chen. NeuroKit2: A python toolbox for neurophysiological signal processing. *Behavior Research Methods*, 53(4):1689–1696, feb 2021.
- [21] Jungwoo Oh, Gyubok Lee, Seongsu Bae, Joon-myung Kwon, and Edward Choi. Ecg-qa: A comprehensive question answering dataset combined with electrocardiogram. *Advances in Neural Information Processing Systems*, 36:66277–66288, 2023.
- [22] Hung Manh Pham, Jialu Tang, Aaqib Saeed, and Dong Ma. Q-heart: Ecg question answering via knowledge-informed multimodal llms. *arXiv preprint arXiv:2505.06296*, 2025.
- [23] B Pyakillya, N Kazachenko, and N Mikhailovsky. Deep learning for ecg classification. *Journal of Physics: Conference Series*, 913(1):012004, oct 2017.
- [24] Andrew Sellergren, Sahar Kazemzadeh, Tiam Jaroensri, Atilla Kiraly, Madeleine Traverse, Timo Kohlberger, Shawn Xu, Fayaz Jamil, Cían Hughes, Charles Lau, et al. Medgemma technical report. *arXiv preprint arXiv:2507.05201*, 2025.
- [25] Aaditya Singh, Adam Fry, Adam Perelman, Adam Tart, Adi Ganesh, Ahmed El-Kishky, Aidan McLaughlin, Aiden Low, AJ Ostrow, Akhila Ananthram, et al. Openai gpt-5 system card. *arXiv preprint arXiv:2601.03267*, 2025.
- [26] Gemini Team, Rohan Anil, Sebastian Borgeaud, Jean-Baptiste Alayrac, Jiahui Yu, Radu Soricut, Johan Schalkwyk, Andrew M Dai, Anja Hauth, Katie Millican, et al. Gemini: a family of highly capable multimodal models. *arXiv preprint arXiv:2312.11805*, 2023.
- [27] Gemma Team, Aishwarya Kamath, Johan Ferret, Shreya Pathak, Nino Vieillard, Ramona Merhej, Sarah Perrin, Tatiana Matejovicova, Alexandre Ramé, Morgane Rivièrè, et al. Gemma 3 technical report. *arXiv preprint arXiv:2503.19786*, 2025.
- [28] Pauli Virtanen, Ralf Gommers, Travis E. Oliphant, Matt Haberland, Tyler Reddy, David Cournapeau, Evgeni Burovski, Pearu Peterson, Warren Weckesser, Jonathan Bright, Stéfan J. van der Walt, Matthew Brett, Joshua Wilson, K. Jarrod Millman, Nikolay Mayorov, Andrew R. J. Nelson, Eric Jones, Robert Kern, Eric Larson, C J Carey, İlhan Polat, Yu Feng, Eric W. Moore, Jake VanderPlas, Denis Laxalde, Josef Perktold, Robert Cimrman, Ian Henriksen, E. A. Quintero, Charles R. Harris, Anne M. Archibald, Antônio H. Ribeiro, Fabian Pedregosa, Paul van Mulbregt, and SciPy 1.0 Contributors. SciPy 1.0: Fundamental Algorithms for Scientific Computing in Python. *Nature Methods*, 17:261–272, 2020.
- [29] Patrick Wagner, Nils Strodthoff, Ralf-Dieter Boussejot, Wojciech Samek, and Tobias Schaeffter. PTB-XL, a large publicly available electrocardiography dataset (version 1.0.3). *PhysioNet*, 2022.
- [30] Zhongwei Wan, Che Liu, Xin Wang, Chaofan Tao, Hui Shen, Jing Xiong, Rossella Arcucci, Huaxiu Yao, and Mi Zhang. Meit: Multimodal electrocardiogram instruction tuning on large language models for report generation. In *Findings of the association for computational linguistics: ACL 2025*, pages 14510–14527, 2025.
- [31] Kai Yang, Massimo Hong, Jiahuan Zhang, Yizhen Luo, Suyuan Zhao, Ou Zhang, Xiaomao Yu, Jiawen Zhou, Liuqing Yang, Ping Zhang, et al. Ecg-lm: Understanding electrocardiogram with a large language model. *Health Data Science*, 5:0221, 2025.
- [32] Yubao Zhao, Jiaju Kang, Tian Zhang, Puyu Han, and Tong Chen. Ecg-chat: A large ecg-language model for cardiac disease diagnosis. In *2025 IEEE International Conference on Multimedia and Expo (ICME)*, pages 1–6. IEEE, 2025.
- [33] Lianmin Zheng, Wei-Lin Chiang, Ying Sheng, Siyuan Zhuang, Zhanghao Wu, Yonghao Zhuang, Zi Lin, Zhuohan Li, Dacheng Li, Eric Xing, et al. Judging llm-as-a-judge with mt-bench and chatbot arena. *Advances in neural information processing systems*, 36:46595–46623, 2023.
- [34] Franklin H. Zimmerman. *ECG Core Curriculum*. McGraw Hill Education, New York, NY, 2023.

A Details of Automated ECG Analysis Pipeline

A.1 Wave Detection and Segmentation Performance

Table 2: Quantitative performances for the ECG segmentation task. The evaluation was conducted on the LUDB dataset [14]. Mean and 95% confidence interval are shown across 3 different train, validation, and test splits. We followed the recommendations of the Association for Medical Instrumentation [2], where it is considered that an onset or an offset is detected correctly if their deviation from the GT annotations does not exceed in the tolerance of 150 ms.

Method	Metric	P Wave		QRS Complex		T Wave	
		P Onset	P Offset	QRS Onset	QRS Offset	T Onset	T Offset
ecgpuwave [5]	Recall	0.872 \pm 0.013	0.872 \pm 0.013	0.993 \pm 0.003	0.992 \pm 0.003	0.890 \pm 0.008	0.848 \pm 0.010
	Precision	0.818 \pm 0.029	0.821 \pm 0.030	0.998 \pm 0.002	0.997 \pm 0.002	0.983 \pm 0.008	0.911 \pm 0.001
NeuroKit2 [20]	Recall	0.969 \pm 0.005	0.967 \pm 0.006	0.861 \pm 0.011	0.796 \pm 0.017	0.781 \pm 0.018	0.722 \pm 0.011
	Precision	0.762 \pm 0.040	0.762 \pm 0.038	0.854 \pm 0.012	0.789 \pm 0.018	0.908 \pm 0.018	0.836 \pm 0.024
UNet3+ [13]	Recall	0.972 \pm 0.004	0.972 \pm 0.004	0.999 \pm 0.001	0.999 \pm 0.001	0.983 \pm 0.006	0.981 \pm 0.006
	Precision	0.942 \pm 0.015	0.944 \pm 0.015	0.999 \pm 0.001	0.999 \pm 0.001	0.993 \pm 0.003	0.991 \pm 0.003
Ours	Recall	0.978 \pm 0.002	0.979 \pm 0.002	1.000 \pm 0.000	1.000 \pm 0.000	0.997 \pm 0.001	0.995 \pm 0.001
	Precision	0.934 \pm 0.036	0.940 \pm 0.036	1.000 \pm 0.000	1.000 \pm 0.000	0.993 \pm 0.005	0.991 \pm 0.005

To rigorously evaluate the wave detection module introduced in Section 3, we utilized the Lobachevsky University Electrocardiography Database (LUDB) [14]. The dataset was randomly partitioned into training, validation, and test sets with an 8:1:1 ratio. To ensure the robustness of our results, this split was repeated using three different random seeds, and we report the mean performance along with the 95% confidence intervals evaluated on the test sets.

Following the recommendation of the Association for the Advancement of Medical Instrumentation (AAMI) [2], a detection was classified as a True Positive if the predicted waveform onset or offset fell within a 150 ms tolerance window of the expert ground truth annotation. Consequently, a GT annotation lacking a corresponding prediction within this 150 ms window was counted as a False Negative, whereas a prediction without a proximate GT annotation was deemed a False Positive.

For performance comparison, we evaluated our pipeline alongside widely used wave detection tools. Specifically, we selected ecgpuwave [5] and NeuroKit2 [20] as representative traditional signal processing methods. To isolate the effect of our post-processing module, we also included the raw UNet3+ [13] model as a deep learning baseline. Finally, Ours denotes the complete proposed pipeline, which pairs the initial UNet3+ outputs with our context-aware post-processing algorithms.

The quantitative results are detailed in Table 2. Overall, the deep learning-based approaches significantly outperformed the traditional signal processing methods. Notably, our complete pipeline (Ours) achieved near-perfect segmentation for QRS complexes (Recall and Precision of 1.000).

When comparing Ours to the raw UNet3+, the application of our post-processing algorithms consistently improved Recall across the waveforms. However, we observed a slight decline in P wave Precision (*e.g.*, from 0.942 to 0.934 for P Onset). It is crucial to note that this statistical drop is an artifact of the LUDB annotation policy rather than an algorithmic failure. Specifically, LUDB systematically omits annotations for non-conducted P waves or P waves occurring during atrioventricular (AV) dissociation. Because our pipeline is explicitly designed to target and recover these unannotated but visually present P waves, the strict evaluation framework categorizes these correct physiological detections as False Positives, thereby artificially lowering the Precision score.

To visually demonstrate this phenomenon, Figure 3 illustrates a representative segment. In the plots, the expert GT annotations are indicated by semi-transparent background masks (*e.g.*, red for QRS complexes and blue for T waves), while the model’s predictions are represented by the corresponding colored segments of the ECG signal itself. The circled regions highlight clear, visually distinct P waves that completely lack GT annotations in the LUDB dataset (indicated by the absence of shaded masks). As shown in the top panel, the raw UNet3+ model strictly adheres to the learned annotation patterns and fails to detect these unannotated P waves. In contrast, the bottom panel demonstrates that our post-processing module successfully recovers and delineates these P waves. Because these

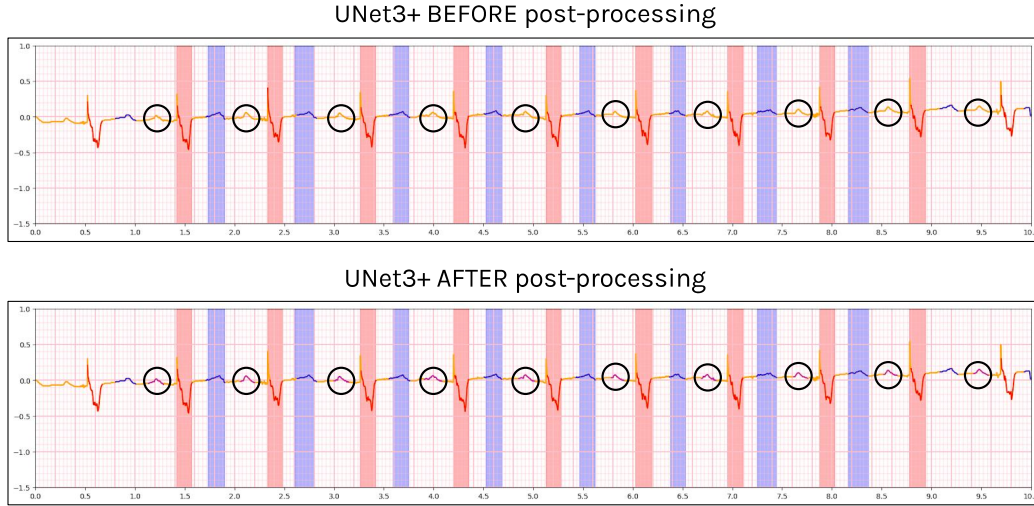


Figure 3: Comparison of P wave detection before (top) and after (bottom) post-processing. Shaded backgrounds indicate GT annotations, while colored signals show predictions. Our pipeline correctly identifies the unannotated P waves (circled), which are penalized as False Positives due to the missing GT.

valid detections do not have matching GT masks, they are strictly penalized as False Positives under the evaluation criteria, resulting in an artificial drop in Precision.

A.2 Diagnostic Logic Diagrams for 17 Core Diagnoses

The 17 core diagnoses evaluated in our benchmark comprehensively cover a wide spectrum of common and critical cardiac abnormalities. To ensure a balanced and clinically representative evaluation, the diagnoses are systematically categorized into six major clinical groups:

- **AV Block (3)**: First Degree AV Block (1AVB), Second Degree AV Block (2AVB), Third Degree AV Block (3AVB)
- **Conduction Disturbance (4)**: Complete Left Bundle Branch Block (CLBBB), Complete Right Bundle Branch Block (CRBBB), Left Anterior Fascicular Block (LAFB), Left Posterior Fascicular Block (LPFB)
- **Hypertrophy (2)**: Left Ventricular Hypertrophy (LVH), Right Ventricular Hypertrophy (RVH)
- **Ectopic Beat (2)**: Premature Atrial Complex (PAC), Premature Ventricular Complex (PVC)
- **Myocardial Infarction (3)**: Anterior Myocardial Infarction (AMI), Inferior Myocardial Infarction (IMI), Lateral Myocardial Infarction (LMI)
- **Ischemia (3)**: Anterior Ischemia (ISCAN), Inferior Ischemia (ISCIN), Lateral Ischemia (ISCLA)

To support the selection of these 17 core diagnoses, we analyzed their prevalence within the two source datasets. Based on the Diagnostic SCP-codes used in the human-annotated PTB-XL dataset, Figure 4 illustrates the distribution of diagnostic labels across both PTB-XL and MIMIC-IV-ECG. In these histograms, the diagnoses directly evaluated by our benchmark are highlight in coral. We also highlight diagnoses in light coral that, while not explicitly listed among the 17 core categories, can be logically derived from them. For instance, an “inferolateral myocardial infarction” can be indirectly inferred through the combination of inferior and lateral MI criteria. Consequently, the 17 core diagnoses directly cover 56.05% of the samples in PTB-XL and 82.03% in MIMIC-IV-ECG. When incorporating the indirectly derivable conditions, the comprehensive coverage expands significantly to 76.85% for PTB-XL and 96.18% for MIMIC-IV-ECG. This high prevalence suggests that our benchmark evaluates highly clinically impactful and frequently encountered conditions in real-world settings.



Figure 4: Prevalence of diagnostic labels in the PTB-XL (left) and MIMIC-IV-ECG (right) datasets. Diagnoses directly covered by the 17 core logic diagrams of **ECG-Reasoning-Benchmark** are highlighted in coral, while conditions that can be indirectly derived from these core diagnoses are highlighted in light coral.

The complete set of hierarchical logic diagrams for the 17 core ECG diagnoses is presented in Figure 6–21. Note that these diagrams illustrate not only the sequence of clinical findings but also the specific grounding elements, such as wave, lead, and measurement grounding, required for each finding, reflecting the exact step-by-step evaluation structure of **ECG-Reasoning-Benchmark**.

B Dataset Statistics

Table 3 summarizes the overall characteristics of **ECG-Reasoning-Benchmark** derived from both PTB-XL and MIMIC-IV-ECG. Specifically, the table details the total number of unique ECG recordings (2, 868 for PTB-XL and 3, 316 for MIMIC-IV-ECG), the distribution of positive (+) and negative (–) cases evaluated through multi-turn interactions, and the vast scale of total question-answering (QA) pairs (24, 097 and 27, 025, respectively). Notably, the evaluation loops require an average of approximately 8 reasoning turns per case (7.81 for PTB-XL and 8.05 for MIMIC-IV-ECG), highlighting the multi-step complexity of our benchmark.

Table 3: Overall statistics of **ECG-Reasoning-Benchmark** derived from the PTB-XL and MIMIC-IV-ECG datasets

Source Dataset		PTB-XL	MIMIC-IV-ECG
# of Unique ECGs		2,868	3,316
# of Cases (Multi-turn)	+	1,377	1,655
	-	1,707	1,704
# of Total QA pairs		24,097	27,025
Avg. reasoning turns		7.81	8.05

To further illustrate the structural depth of our evaluation framework, Table 4 presents the detailed breakdown of cases for each of the 17 core diagnoses. In the table, the specific number of cases allocated to each unique reasoning path is detailed in the “\$ Per Reasoning Path” column, where counts are separated by a vertical pipe (|). To ensure a balanced and robust evaluation, we set a baseline target of 100 positive (+) and 100 negative (-) cases for each diagnoses per dataset. Crucially, we prioritized a strictly uniform distribution of cases across all valid reasoning paths to prevent models from exploiting superficial shortcuts. Consequently, when the target of 100 was not perfectly divisible by the number of reasoning paths, the total sample size was slightly increased to maintain this exact balance (e.g., sampling 34 cases for each of 3 paths yields 102 total cases). Conversely, certain rare diagnoses (e.g., Second and Third Degree AV Block) contain fewer cases due to their natural scarcity in the source datasets.

C Implementation Details

C.1 Detailed Computation of the Depth Metric

To clarify the computation of the **Depth** metric, we present a hypothetical evaluation scenario based on the logic diagram for Complete Left Bundle Branch Block (CLBBB) described in Figure 9. Specifically, suppose a positive CLBBB sample that follows the reasoning path where all four sequential findings are present (i.e., Yes \rightarrow Yes \rightarrow Yes \rightarrow Yes). According to the logic diagram, diagnosing this specific presentation requires the model to successfully navigate four distinct finding loops.

For each loop, the model undergoes the 4-step verification sequence: Criterion Selection (Step 1), Finding Identification (Step 2), ECG Grounding (Step 3), and Diagnostic Decision (Step 4). Step 3 is fractionally scored based on the number of required grounding sub-tasks (N). Suppose a model exhibits the following performance during the evaluation:

- **Finding Loop 1 (Prolonged QRS duration):** This finding requires $N = 2$ grounding sub-tasks (Wave and Measurement Grounding). The model correctly answers Step 1 and Step 2. In Step 3, it correctly identifies the temporal segment (Wave Grounding) but selects wrong value range (Measurement Grounding). Upon this incorrect response, the evaluation for Loop 1 terminates.
 - **Depth Score:** 1 (Step 1) + 1 (Step 2) + 1/2 (Step 3) = 2.5
 - Then, the exact ground-truth history for Loop 1 is explicitly injected into the prompt before proceeding to Loop 2.
- **Finding Loop 2 (Dominant S waves in V1 and V2):** This finding requires $N = 1$ grounding sub-task (Wave Grounding). The model perfectly navigates this loop, passing Steps 1, 2, and 3, and successfully determining that “further findings are required” in Step 4.
 - **Depth Score:** 1 (Step 1) + 1 (Step 2) + 1/1 (Step 3) + 1 (Step 4) = 4.0
 - Then, the evaluation naturally proceeds to Loop 3.
- **Finding Loop 3 (Positive monophasic QRS without Q waves in lateral leads):** This finding requires $N = 2$ grounding sub-tasks (Lead and Wave Grounding). The model correctly selects the diagnostic criterion (Step 1) but incorrectly claims that the finding is absent in the current ECG (Step 2).

Table 4: Detailed case distribution for the 17 core diagnoses in **ECG-Reasoning-Benchmark**. The table outlines the total number of positive (+) and negative (−) cases, the number of distinct reasoning paths for each outcome, and the specific stratification of cases across these paths for both PTB-XL and MIMIC-IV-ECG source datasets.

Dx	# Reasoning Paths		PTB-XL		MIMIC-IV-ECG	
		# Cases	#	Per Reasoning Path	# Cases	# Per Reasoning Path
1AVB	+	1	100	100	100	100
	−	2	100	11 89	100	50 50
2AVB	+	1	3	3	49	49
	−	2	100	50 50	100	50 50
3AVB	+	2	9	0 9	100	50 50
	−	3	102	34 34 34	102	34 34 34
CLBBB	+	2	100	50 50	100	50 50
	−	4	100	25 25 25 25	100	25 25 25 25
CRBBB	+	2	100	15 85	100	50 50
	−	4	100	4 18 39 39	100	25 25 25 25
LAFB	+	1	100	100	100	100
	−	4	102	18 28 28 28	100	25 25 25 25
LPFB	+	1	31	31	100	100
	−	4	101	8 15 39 39	100	25 25 25 25
PAC	+	1	100	100	100	100
	−	2	100	50 50	100	50 50
PVC	+	1	100	100	100	100
	−	2	100	50 50	100	50 50
LVH	+	7	100	4 16 16 16 16 16 16	105	15 15 15 15 15 15 15
	−	4	100	25 25 25 25	100	25 25 25 25
RVH	+	3	34	2 4 28	101	33 34 34
	−	3	102	34 34 34	102	34 34 34
AMI	+	2	100	50 50	100	50 50
	−	1	100	100	100	100
IMI	−	2	100	50 50	100	50 50
	−	1	100	100	100	100
LMI	+	2	100	18 82	100	50 50
	−	1	100	100	100	100
ISCAN	+	2	100	43 57	100	50 50
	−	1	100	100	100	100
ISCIN	+	2	100	18 82	100	50 50
	−	1	100	100	100	100
ISCLA	+	2	100	50 50	100	50 50
	−	1	100	100	100	100

– **Depth Score:** 1 (Step 1) + 0 (Step 2) = 1.0

– Then, the true answers for Loop 3 are injected into the prompt, and the process advances to the final loop.

- **Finding Loop 4 (Notched R waves in lateral leads):** This finding requires $N = 2$ grounding sub-tasks (Lead and Wave Grounding). The model passes Steps 1 and 2 but fails the initial Lead Grounding task in Step 3.

– **Depth Score:** 1 (Step 1) + 1 (Step 2) + 0/2 (Step 3) = 2.0

– Then, the evaluation protocol finally terminates.

From this single CLBBB diagnostic sample, four independent, finding-level Depth scores (2.5, 4.0, 1.0, and 2.0) are extracted. Instead of averaging these scores to represent the sample, all four values are added directly to the global dataset pool. For the sake of this isolated example, the final micro-averaged Depth score would be computed as $(2.5 + 4.0 + 1.0 + 2.0) / 4 = 2.375$. In the full evaluation,

this pooling strategy is applied across all samples in the dataset. The resulting micro-average yields the final Depth metric, precisely representing the exact stage a model can successfully reach for any given clinical finding on average.

C.2 Evaluated Models and Access Endpoints

To ensure the reproducibility of our benchmark results, we detail the specific model versions and access endpoints utilized in our experiments. Proprietary models were queried via their respective official APIs, utilizing the following exact model identifiers to prevent version discrepancies:

- **Gemini-2.5-Flash [4]:** gemini-2.5-flash
- **Gemini-2.5-Pro [4]:** gemini-2.5-pro
- **Gemini-3-Flash [26]:** gemini-3-flash-preview
- **GPT-5-Mini [25]:** gpt-5-mini-2025-08-07
- **GPT-5.2 [25]:** gpt-5.2-2025-12-11

For open-weight models, we loaded the officially released model weights directly from the Hugging Face Hub. The specific repository paths are listed below:

- **PULSE (7B) [18]**
 - A multimodal LLM fine-tuned on the ECGInstruct dataset [18], representing the instruction-tuned model for ECGs.
 - **Hugging Face Repository:** PULSE-ECG/PULSE-7B
- **GEM (7B) [15]**
 - A model designed for grounded ECG understanding, trained to link visual features with textual diagnoses.
 - **Hugging Face Repository:** LANSG/GEM
- **ECG-R1 (8B) [12]**
 - A model trained on the ECG-Protocol-Guided-Grounding-CoT dataset [12], employing Reinforcement Learning to enforce a 6-step analysis protocol for structured ECG interpretation.
 - **Hugging Face Repository:** PKUDigitalHealth/ECG-R1-8B-SFT, PKUDigitalHealth/ECG-R1-8B-RL
- **OpenTSLM (3B) [16]**
 - A time-series native language model capable of processing continuous signals directly, trained with Chain-of-Thought rationales.
 - **Hugging Face Repository:** OpenTSLM/llama3b-ecg-flamingo
- **Hulu-Med (7B, 32B) [11]**
 - A series of models optimized for broad biomedical tasks across various modalities, including medical text, 2D/3D images, and videos.
 - **Hugging Face Repository:** ZJU-AI4H/Hulu-Med-7B, ZJU-AI4H/Hulu-Med-32B
- **MedGemma (4B, 27B) [24], MedGemma-1.5 (4B) [24]**
 - Instruction-tuned version of MedGemma, which is a Gemma3 [27] variant optimized for medical text and image comprehension.
 - **Hugging Face Repository:** google/medgemma-4b-it, google/medgemma-27b-it, google/medgemma-1.5-4b-it
- **Qwen3-VL (8B, 32B) [3]**
 - The latest iteration of the Qwen-VL series, known for strong visual reasoning performance.
 - **Hugging Face Repository:** Qwen/Qwen3-VL-8B-Instruct, Qwen/Qwen3-VL-32B-Instruct
- **Llama-3.2-Vision (11B, 90B) [7]**

- Meta’s open-weights multimodal models, providing a robust baseline for general visual understanding.
- **Hugging Face Repository:** meta-llama/Llama-3.2-11B-Vision-Instruct, meta-llama/Llama-3.2-90B-Vision-Instruct

Additionally, **ECG-Reasoning-Benchmark** evaluates the strict logical deduction capabilities of the models rather than their creative text generation. To maintain absolute consistency and eliminate randomness in the evaluation loop, we configured all models for deterministic output. Specifically, the decoding temperature was set to 0 across all generation pipelines. This configuration ensures that each model produces its most probable reasoning path consistently given the ECG context.

C.3 System Prompt Design

You are an expert cardiologist specializing in advanced electrocardiography. You are participating in a rigorous clinical reasoning examination designed to evaluate your ability to interpret ECGs based on formal authoritative guidelines (e.g., AHA/ACC/HRS Recommendations).

****Instructions:****

1. Read the question and the provided options.
2. Analyze the ECG systematically to answer the question.
3. Select the answer from the given options that correspond to the findings ****visible in the ECG image**** or the correct diagnostic criterion requested.
4. When making a decision, you must base your judgment strictly on established diagnostic criteria defined in standard textbooks (e.g., Goldberger, Marriott, or AHA/ACC Guidelines). You must finalize your diagnosis only when sufficient evidence exists, while explicitly acknowledging that further findings are required if only necessary conditions are met.

Figure 5: System prompt provided to the evaluated models

To purely assess the models’ inherent clinical reasoning and minimize variations caused by prompt engineering, we employed a standardized system prompt across all evaluated models. Crucially, this system prompt is deliberately designed to constrain the models to follow a rigorous, textbook-defined reasoning process. By explicitly mandating adherence to established diagnostic criteria (*e.g.*, AHA/ACC guidelines and standard cardiology textbooks) and requiring sufficient visual evidence before finalizing a diagnosis, we ensure that the models are evaluated on their formal deductive logic rather than heuristic guessing or ungrounded pattern matching. The exact prompt used to initialize the expert cardiologist persona in our evaluation loop is provided in Figure 5.

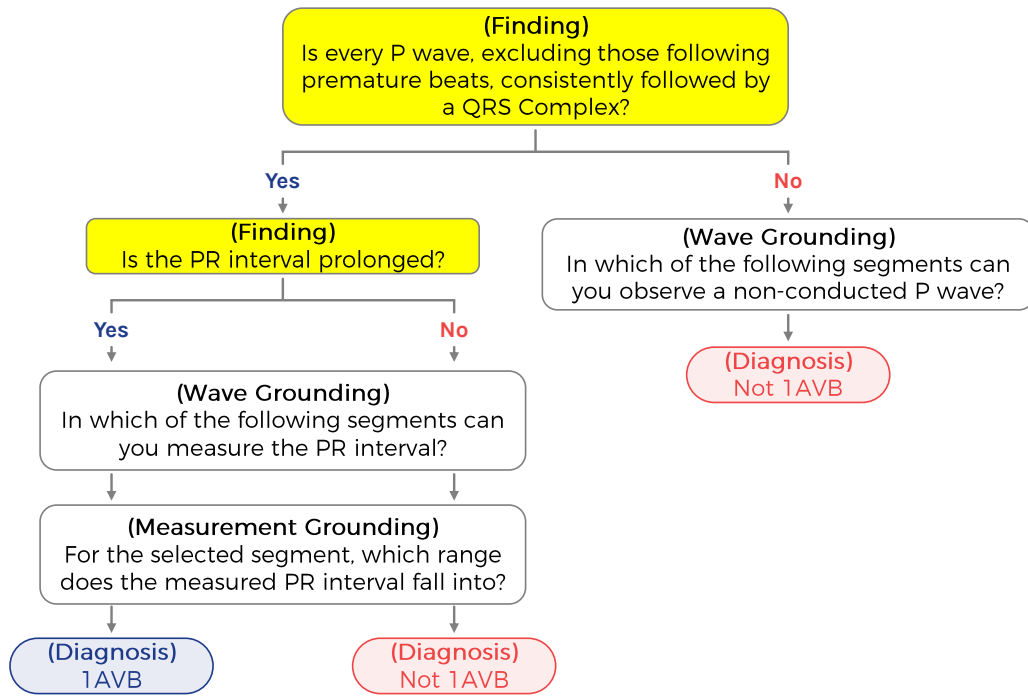


Figure 6: Logic diagram for First Degree AV Block (1AVB)

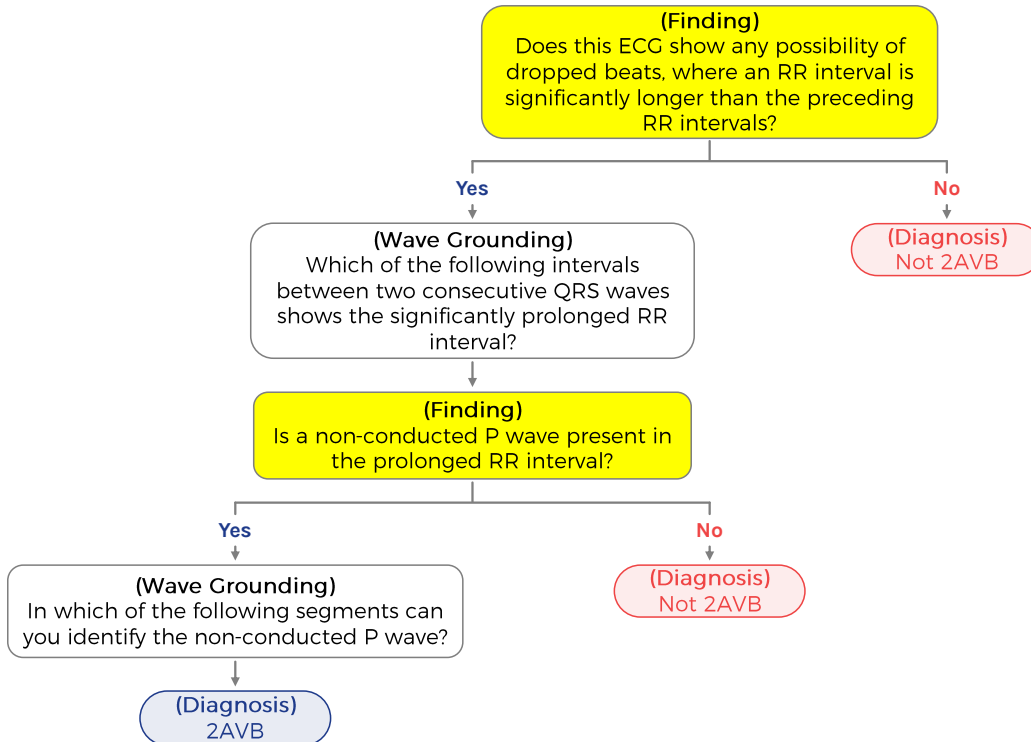


Figure 7: Logic diagram for Second Degree AV Block (2AVB)

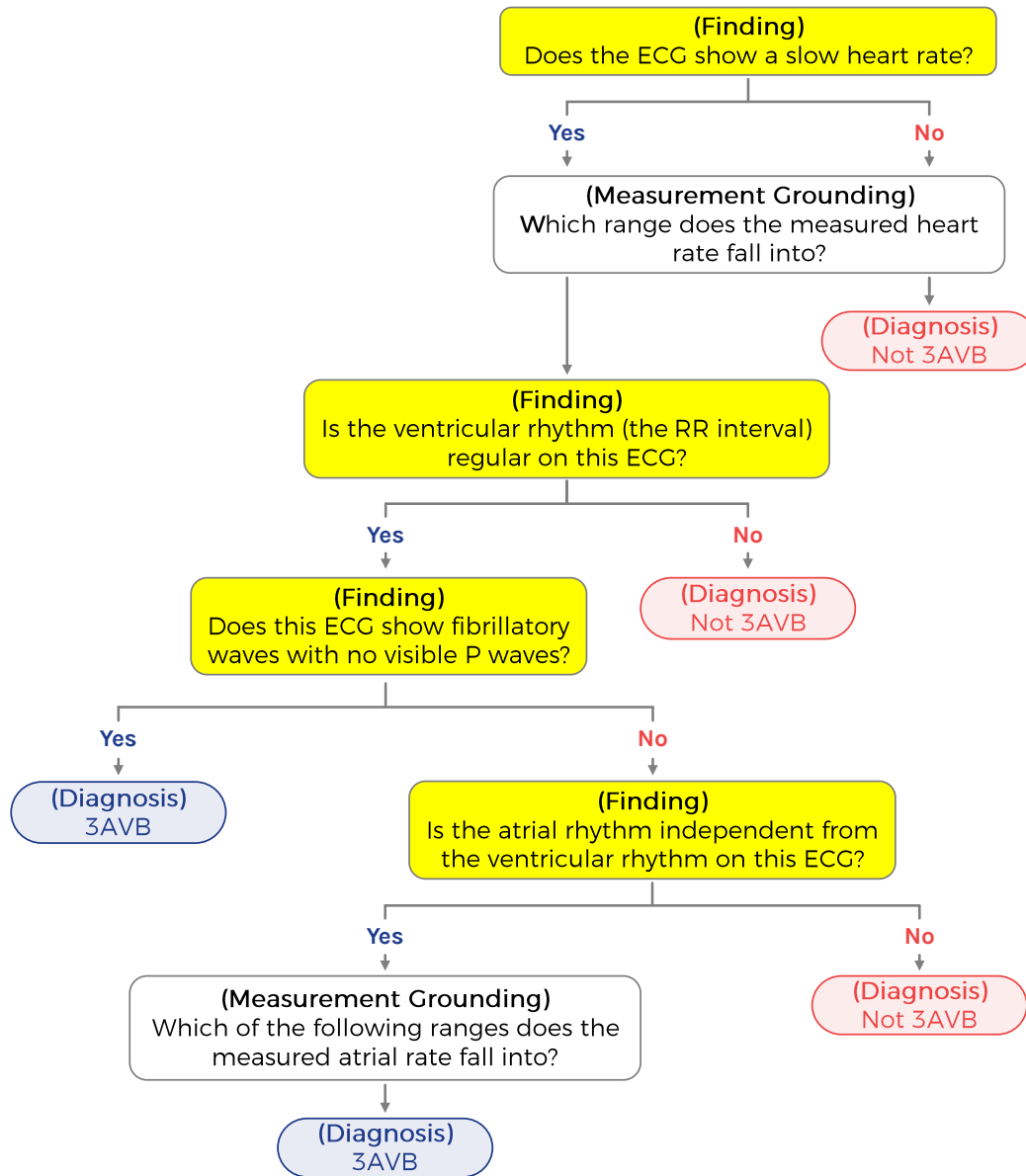


Figure 8: Logic diagram for Third Degree AV Block (3AVB)

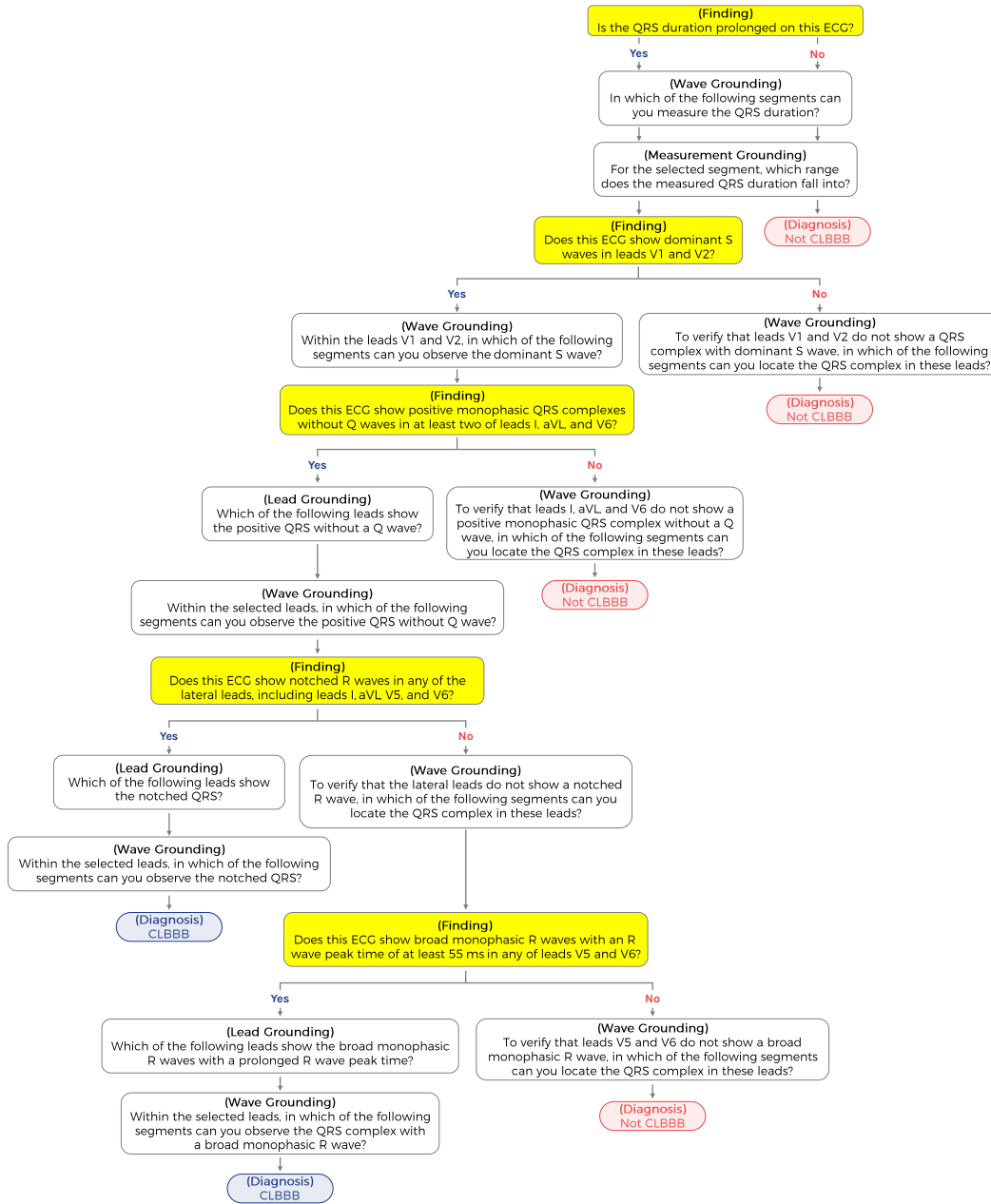


Figure 9: Logic diagram for Complete Left Bundle Branch Block (CLBBB)

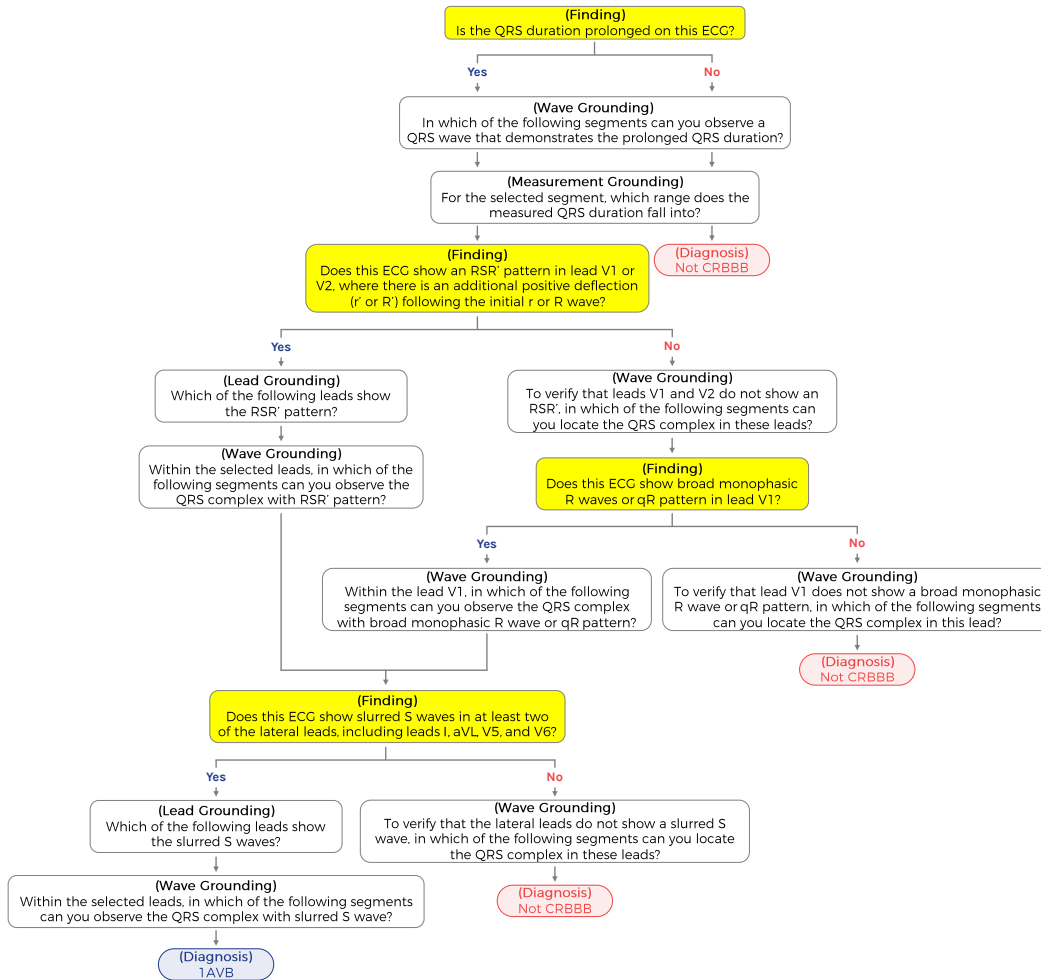


Figure 10: Logic diagram for Complete Right Bundle Branch Block (CRBBB)

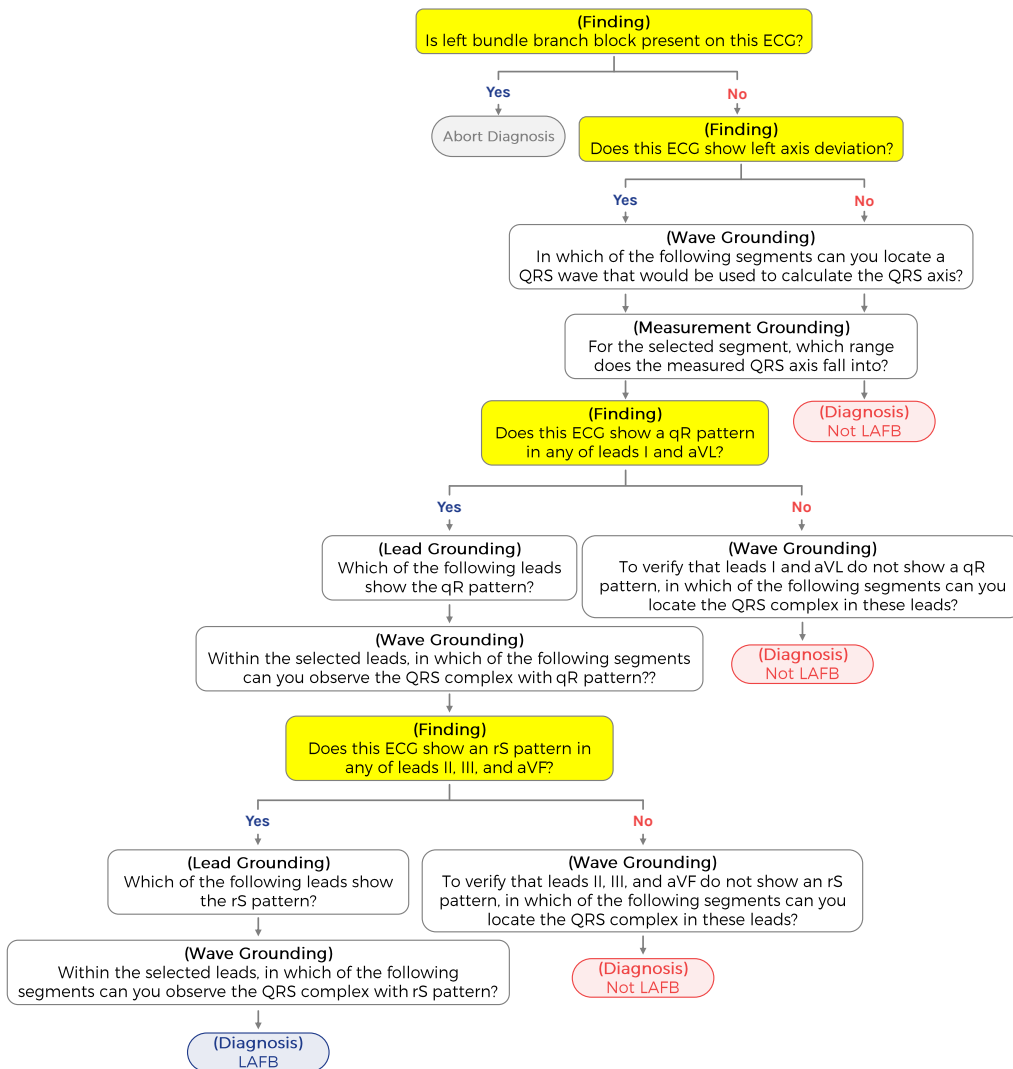


Figure 11: Logic diagram for Left Anterior Fascicular Block (LAFB)

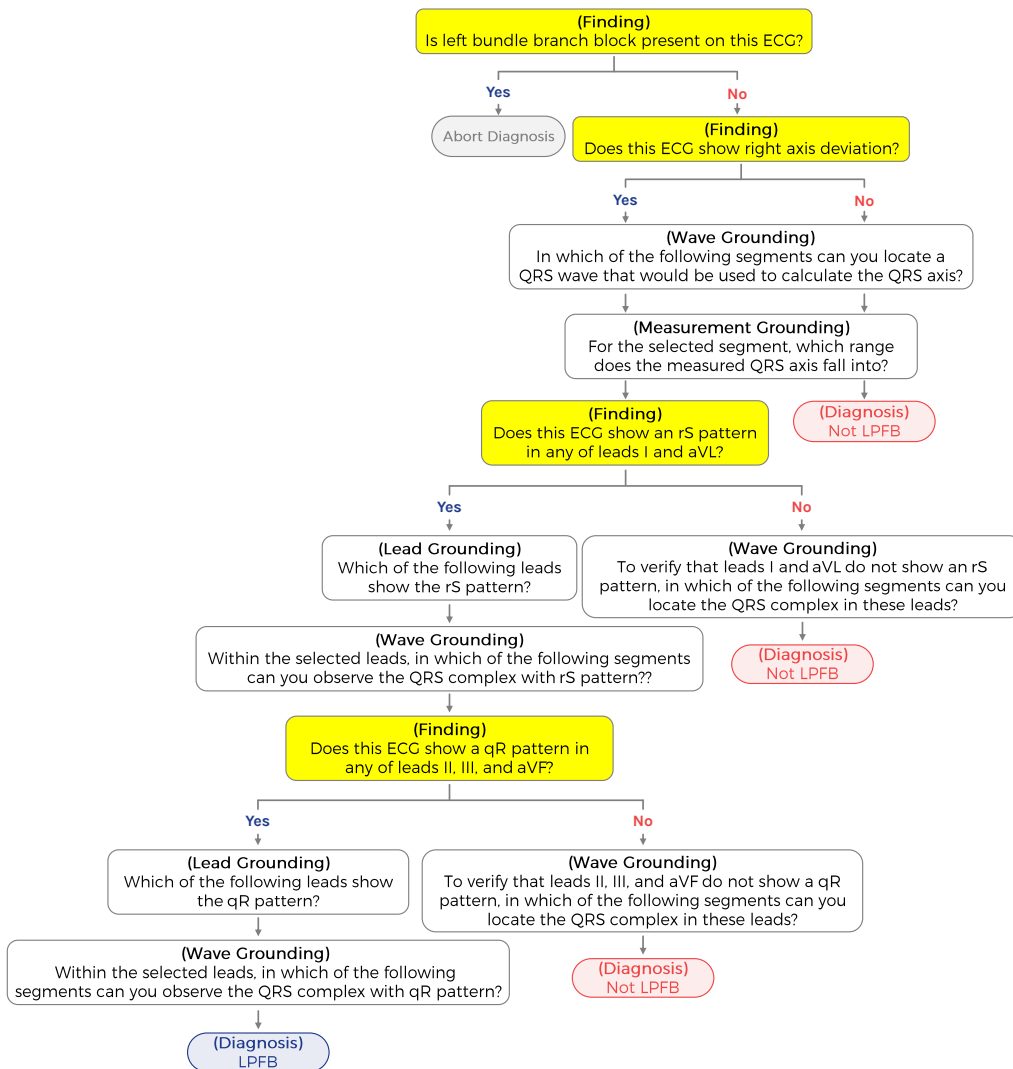


Figure 12: Logic diagram for Left Posterior Fascicular Block (LPFB)

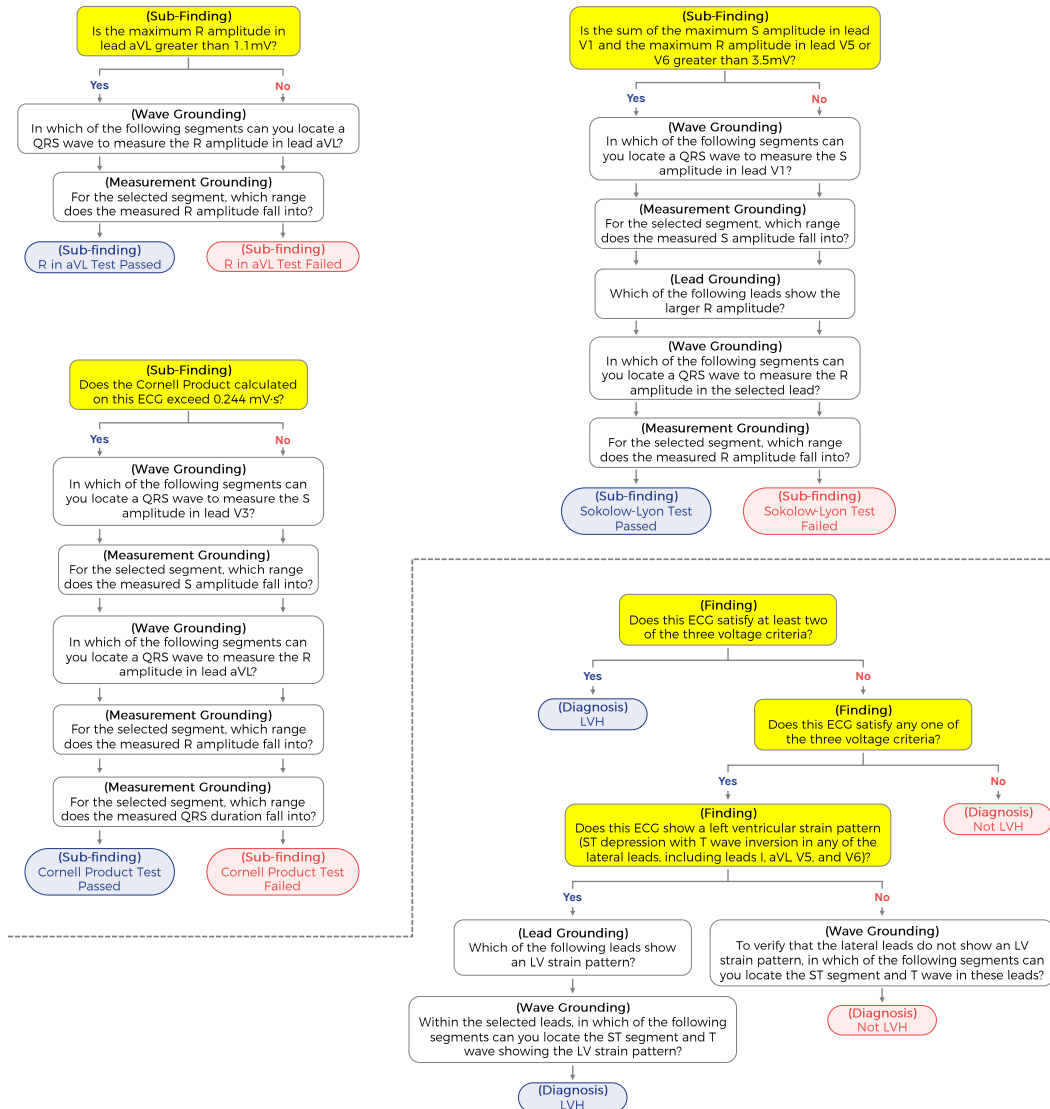


Figure 13: Logic diagram for Left Ventricular Hypertrophy (LVH)

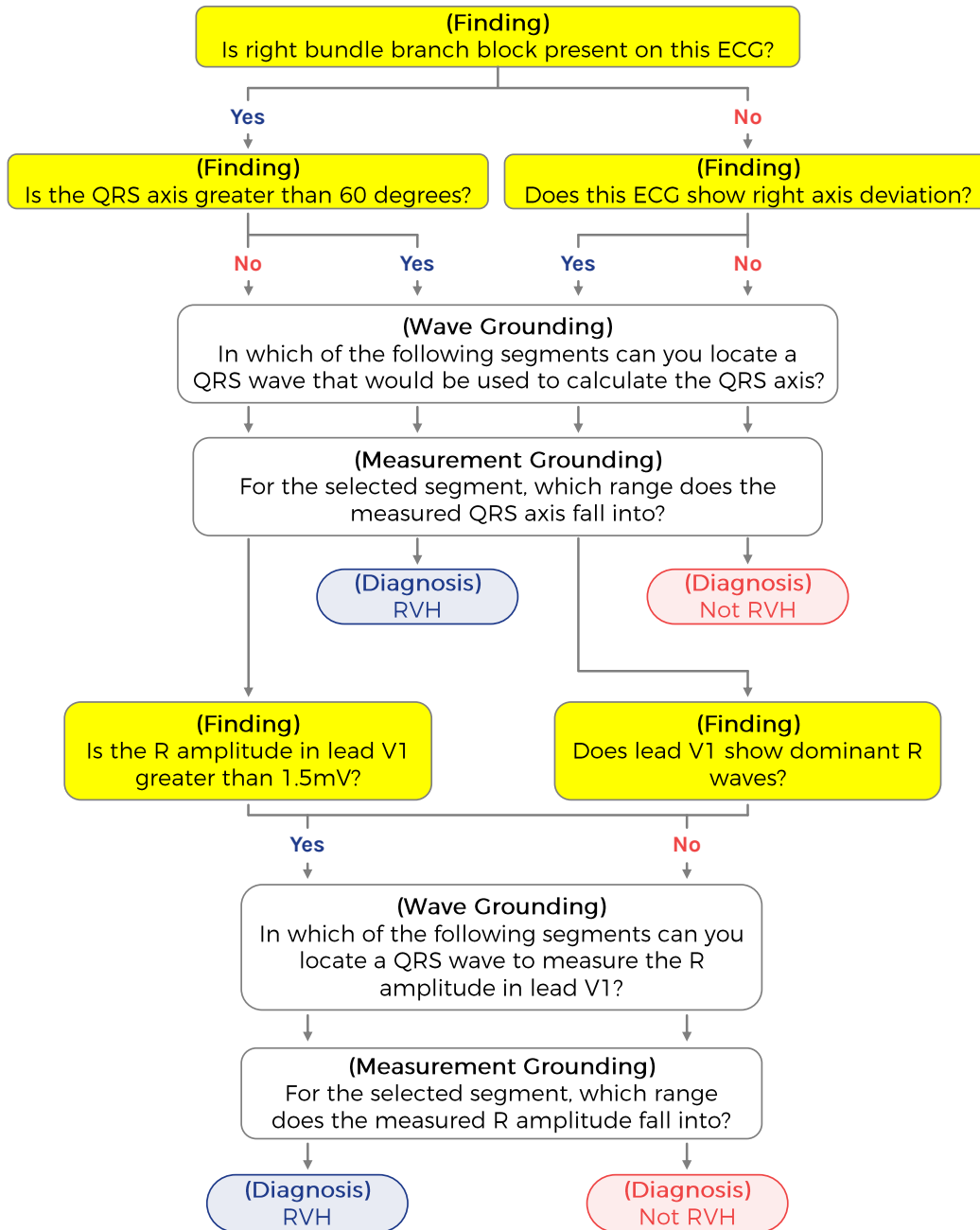


Figure 14: Logic diagram for Right Ventricular Hypertrophy (RVH)

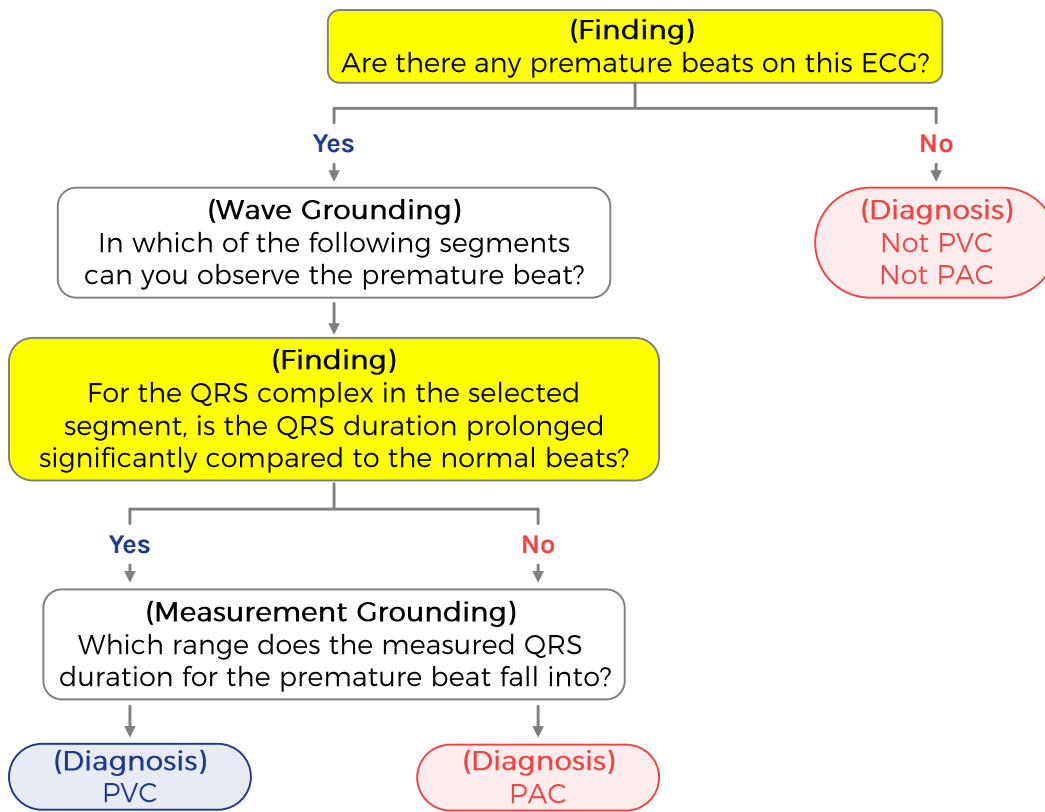


Figure 15: Logic diagram for Premature Atrial Complex (PAC) and Premature Ventricular Complex (PVC)

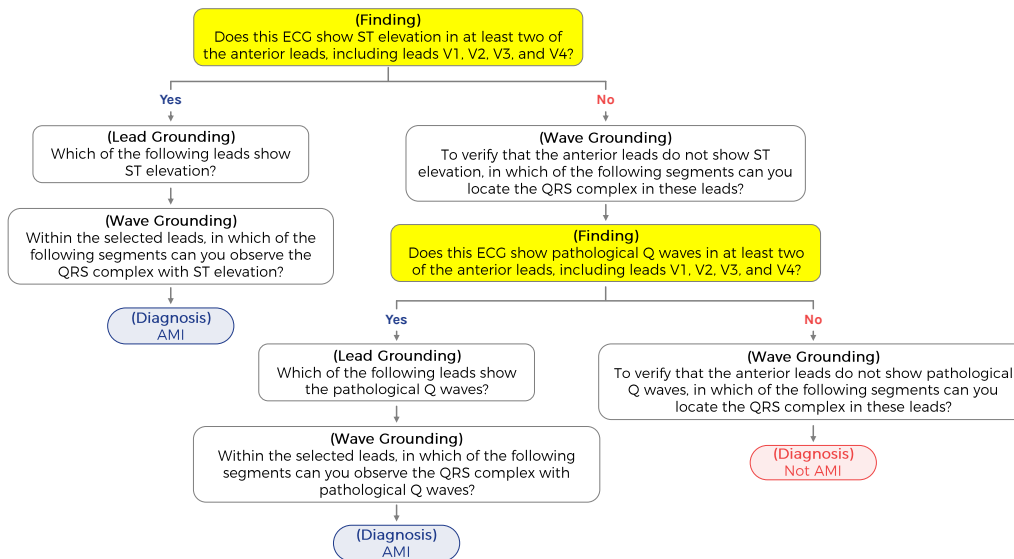


Figure 16: Logic diagram for Anterior Myocardial Infarction (AMI)

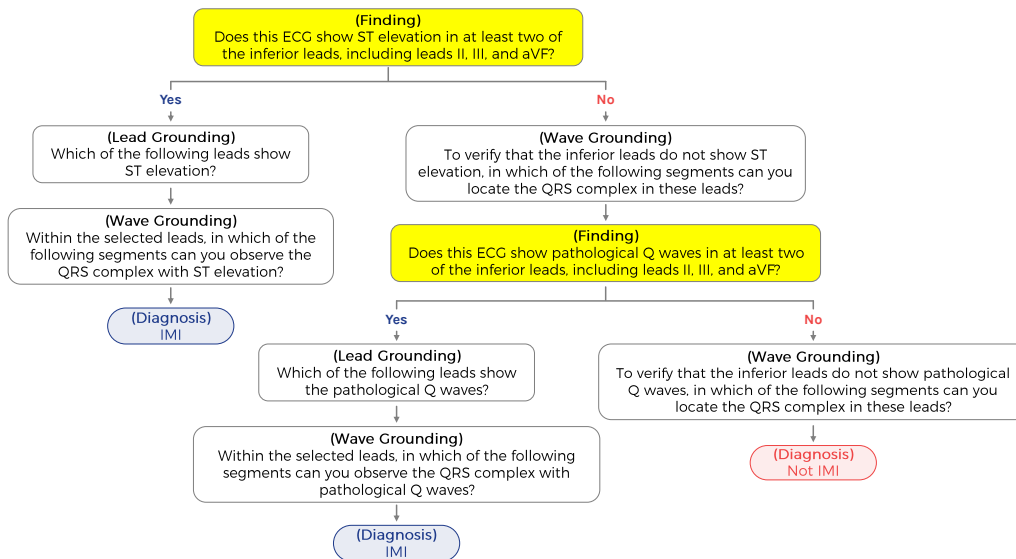


Figure 17: Logic diagram for Inferior Myocardial Infarction (IMI)

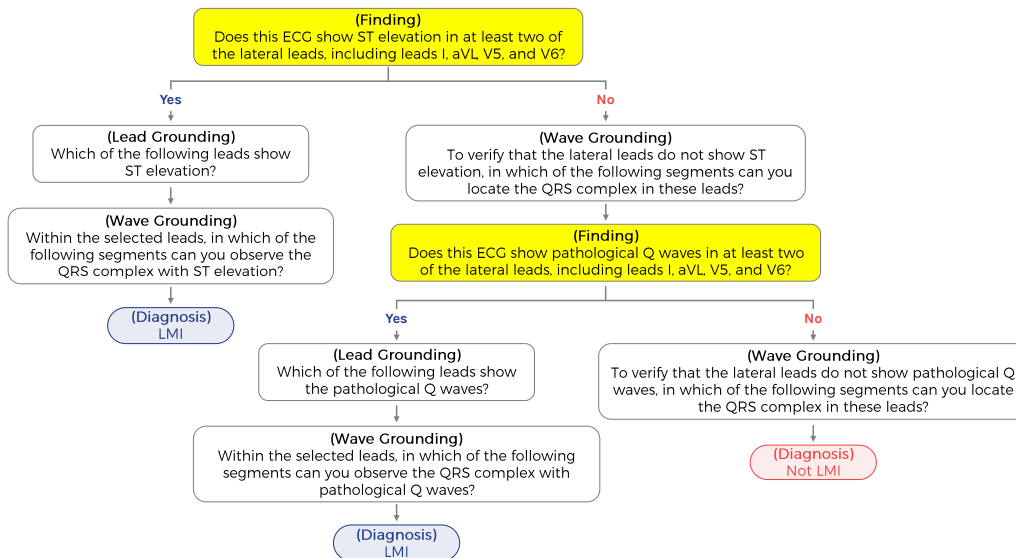


Figure 18: Logic diagram for Lateral Myocardial Infarction (LMI)

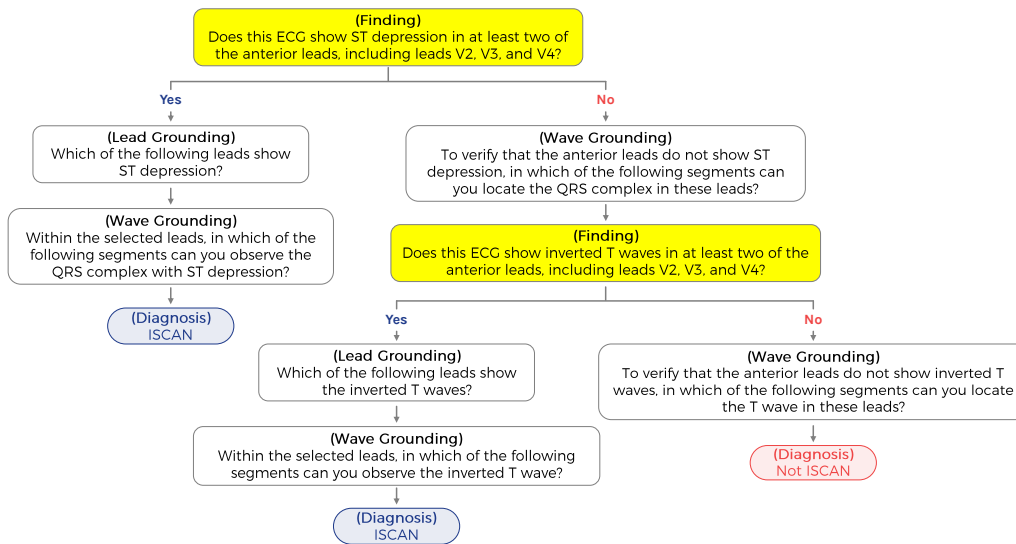


Figure 19: Logic diagram for Anterior Ischemia (ISCAN)

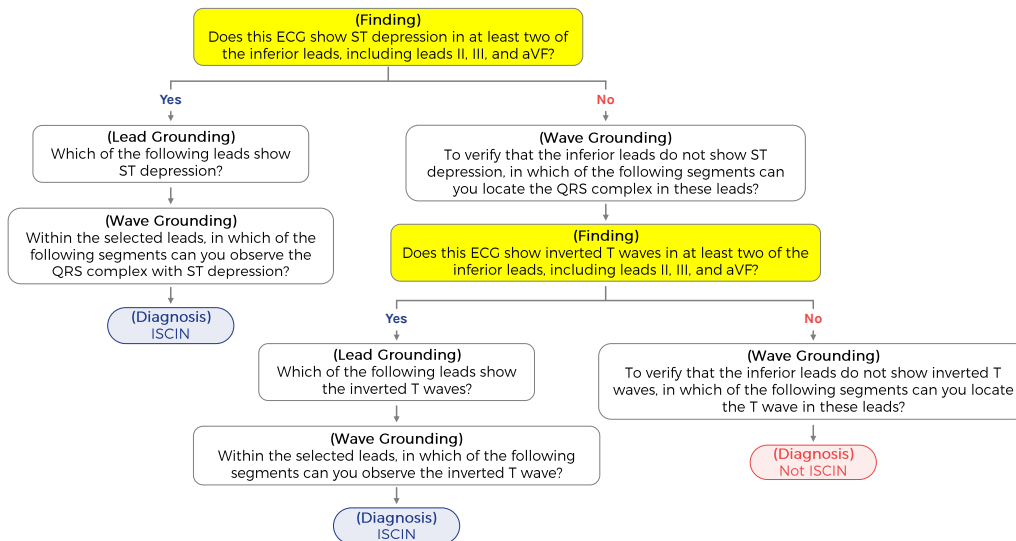


Figure 20: Logic diagram for Inferior Ischemia (ISCIN)

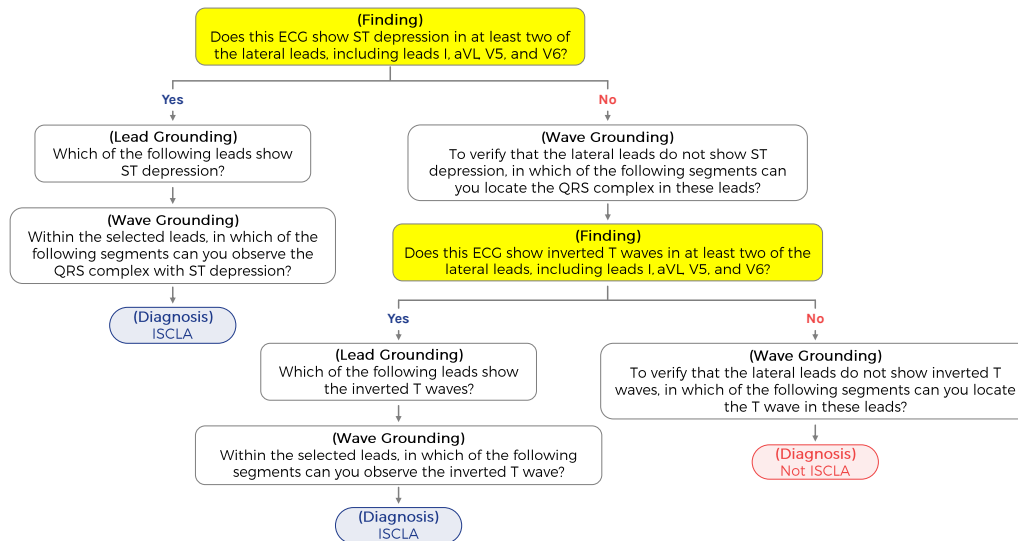


Figure 21: Logic diagram for Lateral Ischemia (ISCLA)